DYNAMICS OF COMPOUND DROPLETS VIA 3D SPECTRAL BOUNDARY ELEMENTS

A Thesis
Submitted to the Graduate Faculty
of the
North Dakota State University
of Agriculture and Applied Science

By

Xiaofeng Qu

In Partial Fulfillment of the Requirements
for the Degree of
MASTER OF SCIENCE

Major Department:
Mechanical Engineering

January 2013

Fargo, North Dakota

North Dakota State University

Graduate School

Title

Dynamics of Compound Droplet Via 3D

Spectral Boundary Elements

By

Xiaofeng Qu

The Supervisory Committee certifies that this **disquisition** complies with North Dakota State University's regulations and meets the accepted standards for the degree of

MASTER OF SCIENCE

SUPERVISORY COMMITTEE:

Dr. Yechun Wang

Chair

Dr. Iskander Akhatov

Dr. Yildirim Bora Suzen

Dr. Alexander Wagner

Approved by Department Chair:

1/7/2013	Dr. Alan Kallmeyer
Date	Signature

ABSTRACT

Compound droplets raise great interests due to their applications in pharmaceutical, cosmetic, and food industry. In spite of the growing demand of theoretical investigation of dynamics of compound droplets from those applications, very limited effort has been contributed in the analytical and/or numerical study of them. In this work, a 3D spectral boundary element method is employed to investigate the dynamics of compound droplets for both concentric and eccentric configurations. A comprehensive investigation has been carried out on the influences of the relative droplet size, relative surface tensions on the two interfaces, relative viscosities of the fluids, and the initial location of the inner droplet, on the deformation, migration, and stability of compound droplets. Two mechanisms of droplet breakup have been observed: (a) the contact of the outer and inner interface and (b) the instability of the inner droplet.

ACKNOWLEDGMENTS

It is my pleasure to take this opportunity to thank the many people who help me during my Master research.

First of all, I must thank my advisor Dr. Yechun Wang, for her guidance, patience, kindness, and motivation. Her experience, knowledge, and critical thinking directed me to solve a lot of difficult problems. She also pushed me to become organized and independent in my research, which is utmost important in my future career.

I would like to acknowledge my committee members, Dr. Iskander S. Akhatov, Dr. Yildirim Bora Suzen, and Dr. Alexander Wagner. Thank you for your valuable time and insight. Your questions and suggestions have led me to a deeper understand of my research.

I would also like to thank Dr. Greg Wettstein, Ph.D. for teaching me how to use the CHPC of CCAST at NDSU. Thanks to Dr. Hideaki Kikuchi who solved the problems during my use of the CHPC.

I wish to thank my parents, Guanghua and Jirong, who have been supporting me all the time. I also want to give my appreciation to my wife Qixin. Her love and encouragement tided me over lots of tough time.

TABLE OF CONTENTS

LIST OF TABLES

LIST OF FIGURES

x

CHAPTER 1. INTRODUCTION

Compound droplets were firstly described by Seifriz [37], who discovered them when he was investigating the double reversal phenomenon of distilled petroleum emulsions. Compound droplets are also called as double emulsions, encapsulated droplets, or globules. They are complex droplets consisted of two droplets: the outer droplet is dispersed in an immiscible continuous phase, while a smaller inner droplet is dispersed in the outer droplet.

1.1. Applications of compound droplets

Compound droplets have raised significant interests because they have a high potential for applications in pharmaceutical, cosmetic, and food industry. In pharmaceutical applications, compound droplets are used to protect, deliver and control the release of the therapeutic molecules engulfed by the inner droplet. Qi et al. used water-in-oil-in-water (W/O/W) double emulsions as a delivery system to improve the oral bioavailability of pidotimod [32]. Wang et al. used W/O/W double emulsions to protect and control the release of liposomes in drug delivery [46]. In cosmetic industry, compound droplets are used to contain active ingredients such as Vitamin C and prolong the release of these ingredients, thus the cosmetic effect can be maximized [1,2]. For application in the food industry, compound droplets are used to encapsulate, protect, and control the release of sensitive and active food components such as vitamin, aroma, and flavor; they are also used to reduce the fat contents in food by substituting the fat with the aquatic phase in the compound droplets [11, 24, 36]. Compound droplets also have the potential to treat waste water. For example, they are employed to remove organic toxicant [7] and heavy metal [6,45] from waste water. Researchers also employed compound droplets as a simplified model of blood cells, to investigate the leukocyte recovery [17,18], the leukocyte adhesion [19,20,27], and the cell epitaxy [41].

1.2. Fabrication of compound droplets

A common process for fabricating compound droplets is a two-step emulsification method [13, 26, 31]. In the first step, water is poured into oil that contains lipophilic emulsifier. This mixture is stirred with high-shear to form fine primary water-in-oil (W/O) droplets that will be the inner droplets. In the second step, the primary droplets are poured into water that dissolves hydrophilic emulsifier. This mixture of the water and the primary droplets is stirred with low-shear to form stable W/O/W compound droplets. Low-shear is employed to prevent the breakup of the primary W/O droplets.

A one-step emulsification process, or phase inversion technique, is also used to generate compound droplets. A large amount of hydrophobic emulsifier together with a small amount of hydrophilic emulsifier is used to form W/O droplets, and then, the W/O droplets are heated to cause part of the emulsions inverted into W/O/W compound droplets [28]. The one-step method is not widely used due to its low effeciency.

Though the above two methods are convenient and conventional to produce compound droplets, they do not have good control over the size and the structure of compound droplets, which is required in many applications. Recently, microfluidics technology is developed to prepare compound droplets that are equally sized. The size and structure of compound droplets can be determined by the flow rate of different phases and the geometry of the microfluidics. Umbanhowar et al. investigated the generation of single droplets in a co-flow device [43]. They found the single droplet size is denpendent on the tube's inner diameter, the inner flow rate, the interfacial tension, and the viscosity and velocity of the contiuous phase. They observed that the diameter of the single droplet was usually more than two times of the tube's inner diameter. By using Umbanhowar theory, Chu et al. developed a capillary

device that consists of two sequential co-flow emulsion generators [9]. They were also able to control the size of the inner and outer droplet by varying the flow rate and tubes' size. By changing these two parameters, they could also control the number of inner droplets. In Chu's study, they could contain the coefficient of variation (CV) of the inner droplet under 2.3% and a better CV of the outer droplet, which was under 1.6%. Utada et al. developed a microcapillary device to generate monodisperse double emulsions [44]. This device was the combination of both co-flow and flow focusing technologies. They were able to control the CV under 1% by varying the flow rate and tubes' size. Some researchers reviewed the new technologies that are able to take good control over the size and structure of compound droplets. Nisisako reviewed the microstructured devices for preparing monodispersed multiple emulsions, which are membrane emulsification, microchannel emulsification, two-dimensional microfluidic device, and three-dimensional coaxial microcapillary device [25]. Shah et al. reviewed the new developments for the controlled fabrication of highly monodispersed emulsions using microfluidics [38].

1.3. On the stability of compound droplets

Emulsion stability refers to the ability of an emulsion to resist change in its properties over time." [23] Researchers have realized the importance of the stability of compound droplets for applications [5, 15]. Due to the instability of compound droplets [14], they cannot be used in practice [8]. Substantive studies have been done to search for the proper combination of emulsifiers to increase the stability of the compound droplet [4, 5, 15]. However, most studies on the stability of compound droplets were experiments, and very limited effort has been contributed in analytical and/or numerical study of the compound droplets.

1.4. Literature review

The first theoretical analysis of compound droplets was done by Torza and Mazon in 1970 [42]. They made the assumption that a three-phase system reached the final equilibrium state when it had a minimum surface free energy. A surface free energy was the summation of the product of the interfacial tension and the interfacial area. Therefore, they believed the three interfacial tensions ($\sigma_{i,j}$, $i \neq j \neq k = $1, 2, 3) were the main factors that determined the equilibrium state. They used three spreading coefficients ($S_i = \sigma_{jk} - \sigma_{ij} - \sigma_{ik}$) to predict the three equilibrium configurations: (1) complete engulfing, when $S_1 < 0$, $S_2 < 0$, and $S_3 > 0$; (2) partial engulfing, when $S_1 < 0$, $S_2 < 0$, and $S_3 < 0$; (3) nonengulfing, when $S_1 < 0$, $S_2 > 0$, and $S_3 < 0$. They also conducted a series of experiments to examine different systems that consisted of various combinations of three phases. Their results generally proved the theoretical prediction. However, they did not consider the effect of the dynamics of fluids in their theoretical studies.

Sadhal and Johnson gave out a dynamic theoretical analysis of the translation of liquid drops or gas bubbles that were partially coated with a thin film of surfactant using the lubrication-theory approximation [34]. In their study, they investigated a creeping flow past drops or bubbles and the internal vortex that was generated by the motion of the drops or bubbles. However, they limited their investigation on the spherical droplets, due to their assumption that the surface tension dominates over the viscous forces. They also only considered the situation that the outer droplet was a stagnant surfactant cap.

Rushton and Davies analytically investigated the motion of the compound droplets in a slow flow [33]. They were interested in the drag coefficient and terminal settling velocity of the compound droplets, because these parameters were the main factors

4

that determined the performance of the membrane separation apparatus. They considered the encapsulated droplet and surrounding membrane to be always spherical.

Stone and Leal were the first researchers that theoretically investigated the breakup of the double emulsions [40]. They employed both analytical and numerical methods in their study. They used a small deformation theory to study the behavior of the double emulsions that were less deformable and a boundary integral method to study the behavior of the double emulsions that had finite deformation. In their study, they investigated a wide range of parameters that could influence the deformation and breakup of double emulsions. These parameters included the flow type (3D uniaxial extensional flow and 3D biaxial extension flow), the inner droplet size, the viscosity ratios, and the interfacial tension ratio. They observed that the uniaxial flow deforms the outer droplet into a prolate shape and the inner droplet into a oblate shape. They found that the increase of the inner droplet size decreases the critical capillary number, and so does the increase of the inner viscosity ratio. They also concluded two mechanisms of double emulsions breakup. One was that double emulsions are stretched by the outer flow until they break up; the other was that the two interfaces contact each other, which causes the double emulsions to break up, even though they are only modestly deformed. However, Stone and Leal only focused on the investigation of concentric double emulsions, and did not investigate eccentric double emulsions. Also, as they have mentioned, they did not fully investigate the viscosity ratios and surface tension ratio.

Smith et al. applied a level set method to investigate the breakup of compound droplets in a shear flow [39]. They shut down the shear flow when the length of the outer droplet was 6 times of the initial radius and allowed the surface tension recover the compound droplets. During the recover process, they discovered that the compound droplets might relax to their initial shape or break up. It is found that

when compound droplets break up, their final configuration is dependent on the flow strength and the surface tension of both inner and outer droplets.

The first theoretical study on the eccentric double emulsion droplets was done by Sadhal and Oguz in 1985 [35]. In their study the compound droplets initially eccentric were placed in a uniform flow with velocity U. Relative motion between inner and outer droplets were taken into consideration. However, the droplets were nearly non-deformable.

There were some other analytical studies concerning the oscillations and stability of compound droplets [12, 21, 22].

1.5. Objectives of this study

The objectives of this paper are to investigate the effect of the size ratio, surface tension ratio, and viscosity raitos on the behavior and stability of concentric compound droplets that are freely suspended in a 2D extensional flow. We also study the behavior of eccentric compound droplets when their inner droplet is placed in different locations inside the outer droplet. We derive the boundary integral equations and employ a 3D spectral boundary element method to simulate the above problems.

The numerical method and the corresponding mathematical formulations are presented in Chapter 2. Our numerical schemes are validated in Chapter 3. We investigate the relationships between the deformation as well as the stability of concentric compound droplets and the size ratios, surface tension ratio, and viscosity ratios in Chapter 4. We study the influence of the placement of the inner droplet on the behavior of the eccentric compound droplets in Chapter 5. Finally, we summarize our findings in Chapter 6.

This is the first time that the 3D spectral boundary element method is applied to investigate the dynamics of a compound droplet. Especially, this method is used

to simulate the behavior of an eccentric compound droplet, which has not been fully investigated and is difficult to perform experimentally.

CHAPTER 2. MATHEMATICAL FORMULATION AND NUMERICAL METHOD

In this study, we investigate the behavior of the compound droplets freely suspended in a 2D extensional Stokes flow via a 3D spectral boundary element method. The behavior of the compound droplets is governed by the Stokes equation and the continuity. In this chapter, we define the problem, nondimensionalize the parameters, derive the Boundary Integral Equations (BIEs), and introduce the numerical schemes. During the introduction of the numerical schemes, we address the discretization of the interfaces and solution procedure.

2.1. Definition of the problem

Consider a compound droplet suspended in a third infinite fluid as shown in Fig. 1. For undeformed droplets, the radius of the outer (Fluid 2) and inner (Fluid 1) droplets are a_o and a_i, respectively, where the subscript, o and i, designate outer and inner droplets, respectively. The three fluids are Newtonian fluid and assumed to be incompressible, thus the volumes of both outer and inner droplets are always constant. Fluid 2 is immiscible with Fluid 1 and Fluid 3. Fluid 1 has a viscosity of μ_i and a density of ρ_i, Fluid 2 has a viscosity of μ_o and a density of ρ_o, and Fluid 3 has a viscosity of μ and a density of ρ. The inner interface formed by Fluid 1 and Fluid 2 has a surface tension of γ_i, and the outer interface formed by Fluid 2 and Fluid 3 has a surface tension of γ_o. The compound droplets are freely suspended in a 2D extensional flow. The flow is expressed by $\boldsymbol{u}^\infty = G(x, -y, 0)$, where G is the shear rate. In this work, we study both concentric and eccentric compound droplets. When a compound droplet is concentric, the centers of mass of the outer and inner droplets are coincident and placed at the stagnant point of the flow. The stagnant point is the center point of an axisymmetric flow, where the velocity is zero. When a
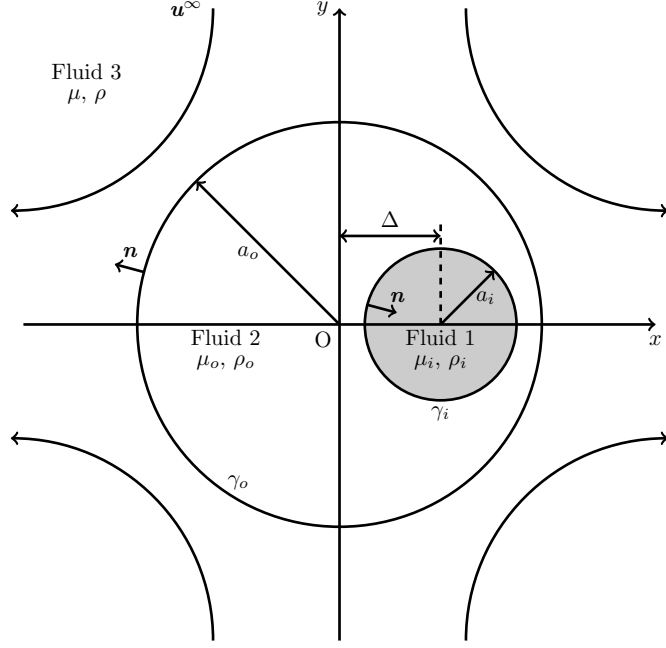
Figure 1: A demonstration of a compound droplet. Fluid 1 is the inner phase, Fluid 2 is the outer phase, and Fluid 3 is the surrounding fluid that disperses the outer droplet. μ is the viscosity, γ is the surface tension, ρ is the density, and a is the radius of an undeformed droplet. The subscripts, o and i, represent the properties for outer and inner droplets, respectively.

compound droplet is eccentric, the centers of mass the outer and inner droplets are separated. The initial location of the center of mass of the outer droplet is always put at the stagnant point. The distance between the centers of mass of the outer and inner droplets is Δ.

In this study, we have made several assumptions: (1) the Reynolds number is low; (2) the three fluids are incompressible; (3) the three fluids have the same densities ($\rho_o = \rho_i = \rho$), so the compound droplets are neutrally buoyant in the fluid flow; (4) the viscosities of the three fluids and surface tensions of the two interfaces are always constant; (5) no surfactant exists.

9

2.2. Nondimensionalization

In this study, the behavior of a concentric compound droplet is determined by ten parameters that are a_o, a_i, γ_o, γ_i, μ, μ_o, μ_i, ρ, ρ_o, ρ_i, and G. Besides these ten parameters, the behavior of a eccentric compound droplet is also determined by the position of the inner droplet. In order to simplify the investigation, we nondimensionalize the parameters. Nondimensionalization has three major advantages. First, it can reduce the number of parameters. Second, using a nondimensional equation, computations can be simplified, for example the inertia term can be neglected in microfluidics due to small Reynolds number. Third, nondimensonalization makes the parameters generalized and applicable for a generic system [49]. In this study, we use the radius of the undeformed outer droplet a_o as the length scale, $a_o G$ as the velocity scale, and $1/G$ as the time scale. The dimensionless parameters are listed below,

$$k = a_i/a_o, \tag{1}$$

$$\lambda_o = \mu_o/\mu, \tag{2}$$

$$\lambda_i = \mu_i/\mu, \tag{3}$$

$$\Gamma = \gamma_i/\gamma_o, \tag{4}$$

$$\beta_o = \rho_o/\rho, \tag{5}$$

$$\beta_i = \rho_i/\rho, \tag{6}$$

$$\delta = \Delta/a_o, \tag{7}$$

$$Ca_o = \frac{\mu G a_o}{\gamma_o}, \tag{8}$$

$$Ca_i = \frac{\lambda_o \mu G a_i}{\gamma_i}, \tag{9}$$

$$Re = \frac{\rho G a_o}{\mu}, \tag{10}$$

where k is the size ratio; λ_o and λ_i are the outer and inner viscosity ratios; Γ is

the surface tension ratios; β_o and β_i are the outer and inner density ratios; δ is the eccentricity; Ca_o and Ca_i are the outer and inner capillary numbers, respectively, the capillary number measures the relative importance of viscous forces and surface tension, thus determines the deformability of a droplet in a given fluid and flow condition; and Re is Reynolds number that is the ratio of inertia forces to viscous forces.

We are interested in the influence of above parameters on the deformation of the compound droplet. The deformation is defined by

$$D = \frac{L - S}{L + S},\tag{11}$$

where L is the longest axis of the droplet and S is the shortest axis.

2.3. Boundary Integral Equation

In this study, all the fluids are governed by Navier-Stokes equation

$$\rho(\frac{\partial \boldsymbol{u}}{\partial t} + \boldsymbol{u} \cdot \nabla \boldsymbol{u}) = -\nabla p + \mu \nabla^2 \boldsymbol{u},\tag{12}$$

where $\boldsymbol{u}$ is the velocity, and p is the dynamics pressure. Due to the small size of compound droplets involved in many industrial processes, the Reynolds number is sufficiently small, and consequently the inertia forces are negligible. Therefore, the inertia terms in the Navier-Stokes equations are neglected, and the flow is governed by Stokes equation

$$\nabla \cdot \boldsymbol{\sigma} \equiv -\nabla p + \mu \nabla^2 \boldsymbol{u} = \boldsymbol{0},\tag{13}$$

where $\boldsymbol{\sigma}$ represents the stress tensor. The Stokes equation is supplemented by the

continuity for incompressible flow

$$\nabla \cdot \boldsymbol{u} = 0. \tag{14}$$

In this study, the boundary conditions for the velocity $\boldsymbol{u}$ and surface stress $\boldsymbol{f}$ on the inner interface are

$$\boldsymbol{u}_1 = \boldsymbol{u}_2, \tag{15}$$

$$\Delta \boldsymbol{f}_{12} \equiv \boldsymbol{f}_1 - \boldsymbol{f}_2 = \gamma_o (\nabla \cdot \boldsymbol{n}) \boldsymbol{n}, \tag{16}$$

while the boundary conditions on the outer interface are given by

$$\boldsymbol{u}_2 = \boldsymbol{u}_3, \tag{17}$$

$$\Delta \boldsymbol{f}_{32} \equiv \boldsymbol{f}_3 - \boldsymbol{f}_2 = \gamma_i (\nabla \cdot \boldsymbol{n}) \boldsymbol{n}. \tag{18}$$

Here the subscripts 1, 2, and 3 designate the velocity and the surface stress evaluated in fluids 1, 2, and 3. The surface stress is defined by

$$\boldsymbol{f} = \boldsymbol{\sigma} \cdot \boldsymbol{n}, \tag{19}$$

where $\boldsymbol{n}$ is the unit normal. We choose $\boldsymbol{n}$ to point into Fluid 1 on the inner interface and into Fluid 3 on the outer interface. Eqs. 15 and 17 constrain the velocity on the interfaces to be continuous, and Eqs. 16 and 18 indicate that the stress jump on the interface is due to the surface tension.

The inner Boundary Integral Equation (Eq. 20) relates the velocity $\boldsymbol{u}$ at each point $\boldsymbol{x}_0$ along the boundary S_B by the surface integral of the stress and velocity over all the points $\boldsymbol{x}$ on the same boundary. It expresses the flow field inside a boundary

12

S_B shown in Fig. 2a. The normal vector $\boldsymbol{n}$ points into the domain surrounded by the boundary S_B.

$$\boldsymbol{u}(\boldsymbol{x}_0) = -\frac{1}{4\pi\mu} \int_{S_B} (\boldsymbol{S}\cdot\boldsymbol{f} - \mu\boldsymbol{T}\cdot\boldsymbol{u}\cdot\boldsymbol{n})dS. \tag{20}$$

In Eq. 20, S_{ij} is the fundamental solution for the velocity of the Stokes equations, and T_{ijk} is the associated stress. They are defined by

$$S_{ij} = \frac{\delta_{ij}}{r} + \frac{\hat{x}_i\hat{x}_j}{r^3}, \; T_{ijk} = -6\frac{\hat{x}_i\hat{x}_j\hat{x}_k}{r^5}, \tag{21}$$

where $\hat{\boldsymbol{x}} = \boldsymbol{x} - \boldsymbol{x}_0$ and $r = |\hat{\boldsymbol{x}}|$. The detailed derivation is done by Pozrikidis in his book [30].

The outer Boundary Integral Equation (Eq. 22) expresses the flow field outside a boundary S_B shown in Fig. 2b. The normal vector $\boldsymbol{n}$ points into the surrounding flow, and $\boldsymbol{u}^\infty$ represents the undisturbed velocity far from the boundary S_B [47].

$$\boldsymbol{u}(\boldsymbol{x}_0) - 2\boldsymbol{u}^\infty(\boldsymbol{x}_0) = -\frac{1}{4\pi\mu} \int_{S_B} (\boldsymbol{S}\cdot\boldsymbol{f} - \mu\boldsymbol{T}\cdot\boldsymbol{u}\cdot\boldsymbol{n})dS. \tag{22}$$

In our study, Fluid 2 is treated as the inner phase bounded by the outer interface and the inner interface. Therefore, the outer Boundary Integral Equation is applied to Fluid 1 and Fluid 3, and the inner Boundary Integral Equation is applied to Fluid 2

$$\boldsymbol{u}(\boldsymbol{x}_0) - 2\boldsymbol{u}^\infty(\boldsymbol{x}_0) = -\frac{1}{4\pi\lambda_i\mu} \int_{S_i} (\boldsymbol{S}\cdot\boldsymbol{f}_1 - \lambda_i\mu\boldsymbol{T}\cdot\boldsymbol{u}\cdot\boldsymbol{n})dS, \tag{23}$$

$$\boldsymbol{u}(\boldsymbol{x}_0) = -\frac{1}{4\pi\lambda_o\mu} \int_{S_i+S_o} (\boldsymbol{S}\cdot\boldsymbol{f}_2 - \lambda_o\mu\boldsymbol{T}\cdot\boldsymbol{u}\cdot\boldsymbol{n})dS, \tag{24}$$

$$\boldsymbol{u}(\boldsymbol{x}_0) - 2\boldsymbol{u}^\infty(\boldsymbol{x}_0) = -\frac{1}{4\pi\mu} \int_{S_i} (\boldsymbol{S}\cdot\boldsymbol{f}_3 - \mu\boldsymbol{T}\cdot\boldsymbol{u}\cdot\boldsymbol{n})dS, \tag{25}$$

13
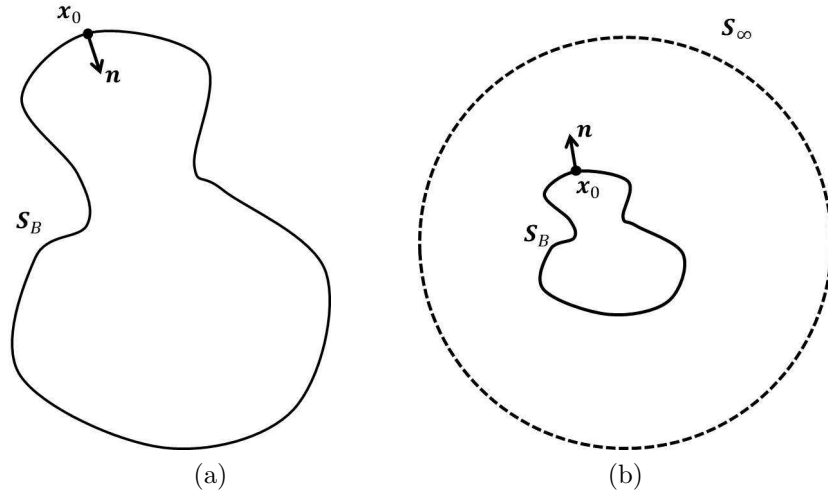
Figure 2: Illustrations for the geometry of the BIEs (Eqs. 20 and 22).

Since only the stress difference on the interface is known, Eq. 24 is subtracted from Eq. 23 and Eq. 25, respectively, to obtain the Boundary Integral Equations for the outer and inner interface

$$
\begin{aligned}
\Omega \boldsymbol{u} - \Omega_o \boldsymbol{u}^\infty = \quad & - \quad \frac{1}{4\pi\mu} \int_{S_o} [S \cdot \Delta \boldsymbol{f}_{23} - (1 - \lambda_o)\mu \boldsymbol{T} \cdot \boldsymbol{u} \cdot \boldsymbol{n}] dS \\
& - \quad \frac{1}{4\pi\mu} \int_{S_i} [S \cdot \Delta \boldsymbol{f}_{12} - (\lambda_i - \lambda_o)\mu \boldsymbol{T} \cdot \boldsymbol{u} \cdot \boldsymbol{n}] dS
\end{aligned} \tag{26}
$$

where Ω and Ω_o are the coefficients for different interfaces, $\Omega = 1 + \lambda_o$ and $\Omega_o = 2$ for the outer interface S_o, and $\Omega = \lambda_i + \lambda_o$, and $\Omega_o = 2\lambda_i$ for the inner interface S_i. Boundary Integral Equations could be used to determine the velocity at any geometric point on the interfaces of the compound droplets.

2.4. Numerical schemes

A three-dimensional spectral boundary element method for interfacial dynamics in Stokes flow is employed to find the numerical solution of the aforementioned

integral equation. The main attraction of our algorithm is that it combines the high accuracy of spectral methods without creating denser systems and possesses the versatility of boundary element methods, i.e. the ability to handle the most complicated geometries, as described in Ref. [48].

2.4.1. Discretization

We use cube projection to discretize the initial spherical shape and create spectral elements. As shown in Fig. 3, the droplet interface is discretized into six spectral elements ($N_E = 6$), while each element is projected to one of the cube surfaces. We discretize each element in two dimentions. The geometry variables are defined using the geometry collocation points (N_G), while the physical variables are defined using basis points (N_B). Those basis points are parameterized points which are the zeros of N_Bth order orthogonal polynomials. The collocation points are used to avoid singularity. J.J.L. Higdon and G.P. Muldowney gave a detailed inroduction of the surface element discretization in their paper [16]. In each element, we have N_B spectral points in one curvilinear direction, thus we have N_B^2 points on each element, $N_E N_B^2$ points on each interface, and totally $2N_E N_B^2$ points for a compound droplet. In addition, an interfacial smoothing scheme and a mesh redistribution strategy have been employed based on work by Wang and Dimitrakopoulas [48].

To determine the N_B number, we conducted a convergence test as shown in Fig. 4. We carried out the convergence test for a a compound droplet of $Ca_o = 0.06$, $k = 0.1$, $\Gamma = 1$, and $\lambda_o = \lambda_i = 1$. The compound droplet is freely suspended in a uniaxial extensional flow. We computed the deformation of a compound droplet using $N_B = 5, 7, 9, 11$, and 13. The relative error in deformation is calculated based on the results of $N_B = 15$. In Fig. 4, the y axis is the relative error in deformation, and the x axis represents the total spectral points number that is calculated by $N = 2N_E N_B^2$. When $N_B = 11$, which is $N = 1452$, the relative error in deformation is in the order
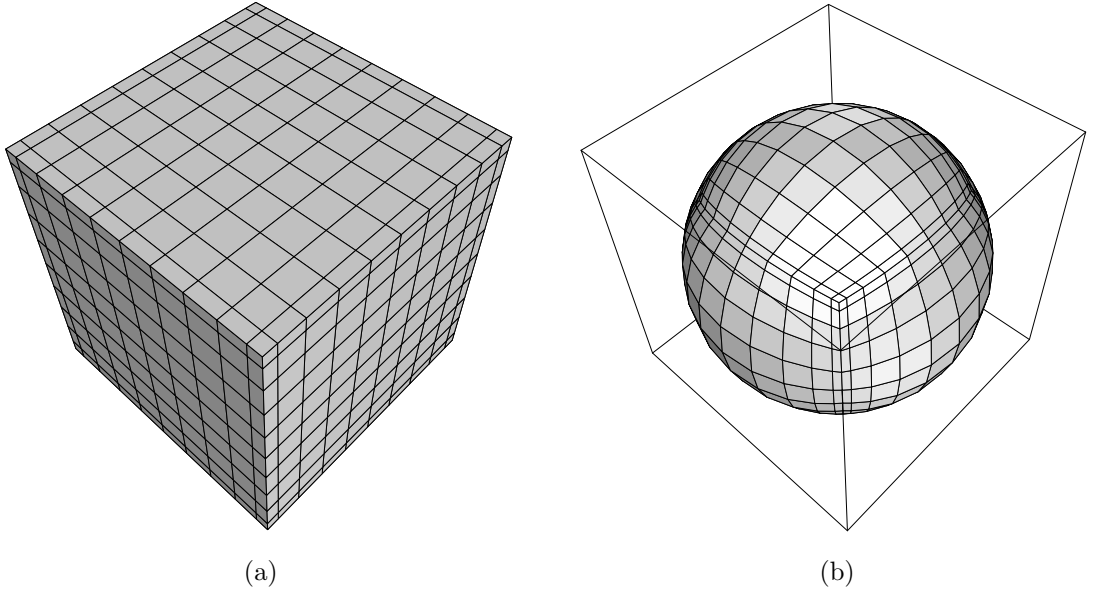
Figure 3: (a) Discretization of a cubic surface; (b) Discretization of a droplet interface via cubic projection.

of 10^{-5}. This error is already negligible, thus, we choose $N_B = 11$ in our study.

2.4.2. Solution procedure

A linear system of algebraic equations $\boldsymbol{u} = \boldsymbol{A}\boldsymbol{f} + \boldsymbol{B}\boldsymbol{u}$ is obtained by substituting the discretized points into the boundary integral equation. The system matrices $\boldsymbol{A}$ and $\boldsymbol{B}$ are defined as integrals of the kernels $\boldsymbol{S}$ and $\boldsymbol{T}$ and the basis functions over the set of the surface elements. These equations are solved via Gauss elimination method by using the routines from the LAPACK system library. The velocity at each point on the interface is obtained, and displacement of each point is determined by solving the kinematic condition at the droplet interface

$$\frac{d\boldsymbol{x}}{dt} = (\boldsymbol{u} \cdot \boldsymbol{n})\boldsymbol{u}, \tag{27}$$

where $\boldsymbol{x}$ is the position vector of a point at the droplet interface, $\boldsymbol{u}$ is the velocity vector of the same point, and $\boldsymbol{n}$ is the unit normal vector. This equation is solved

16
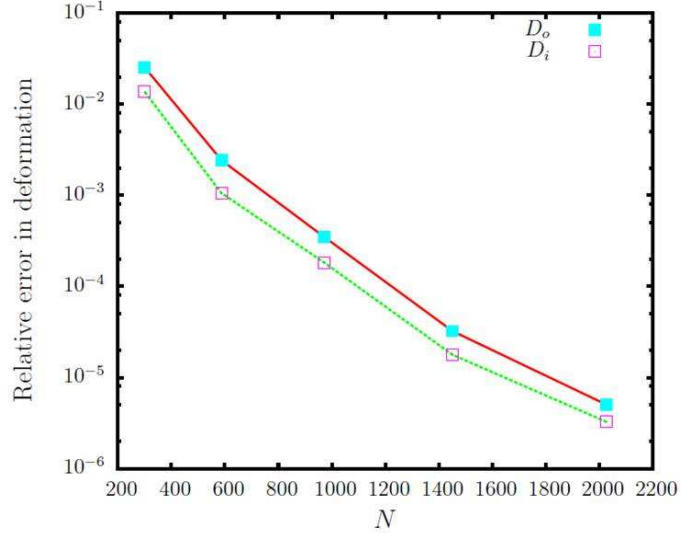
Figure 4: Convergence test with a compound droplet of $Ca_o = 0.06$, $k = 0.1$, $\Gamma = 1$, and $\lambda_o = \lambda_i = 1$. The compound droplet is freely suspended in a uniaxial extensional flow. The N_B number is $N_B = 5$, 7, 9, 11, and 13. The number of the spectral points is calculated by $N = 2N_E N_B^2$.

using a 4th order Runge-Kutta method.

CHAPTER 3. VALIDATION

We validate our numerical schemes by comparing simulation results with the results from Stone and Leal's work [40]. For good precision, Engauge Digitizer is used to digitize figures. We also program in MATLAB using small deformation theory for the purpose of comparison.

The 3D Spectral Boundary Element Method is a fully three dimensional numerical method. By using this method, the interface of the droplet is discretized with spectral elements, which results in high accuracy and exponential convergence. The Small Deformation Theory uses a domain perturbations method to generate analytic solution for the dynamics of a compound droplet. To make this method valid, the compound droplet has to be assumed as nearly spherical, which is realized by low capillary number ($Ca_o \ll 1$ and $Ca_i \ll 1$). The Boundary Integral Method employed by Stone and Leal is a axisymmetric method because of their flow selection. They discretize the interface of droplet with equal-space points or an arclength parametrization method [3].

In Fig. 5a, we present the steady state deformation of compound droplets at different capillary numbers in a 3D extensional flow. The undisturbed flow is $\boldsymbol{u}^\infty = G(-x/2, -y/2, 2z)$. The deformation are calculated for ten values of the outer capillary numbers $Ca_o = 0.01, 0.02, ... , 0.10$. The other parameters are fixed: $\lambda_o = \lambda_i = 1$, $\Gamma = 1$, and $k = 0.5$. The inner capillary number is $0.5Ca_o$ in this case. As shown in Fig. 5a, the square symbols represent the steady state deformation simulated by our 3D spectral boundary element method, and the round symbols represent the deformation generated by Stone and Leal's boundary integral method. The solid lines denote the predictions calculated by small deformation theory that is also derived by Stone and Leal. In Table 1, we present the steady state deformation generated by different methods in a 3D uniaxial flow. The superscripts BEM, BIM,

Table 1: Comparison of steady state deformation generated by Small Deformation Theory (SD), Boundary Element Method (BEM), and Boundary Integral Method (BIM) in a 3D uniaxial flow.

Ca_o	0.01	0.02	0.03	0.04	0.05	0.06	0.07	0.08	0.09	0.10
D_o^{SD}	0.019	0.037	0.056	0.074	0.092	0.110	0.127	0.145	0.162	0.179
D_o^{BEM}	0.019	0.039	0.060	0.082	0.106	0.131	0.158	0.188	0.223	0.266
D_o^{BIM}	0.020	0.040	0.060	0.080	0.106	0.129	0.157	0.190	0.222	0.266
D_i^{SD}	0.0067	0.0133	0.0201	0.0268	0.0336	0.0404	0.0472	0.0541	0.0610	0.0679
D_i^{BEM}	0.0066	0.0130	0.0193	0.0253	0.0310	0.0362	0.0409	0.0449	0.0480	0.0498
D_i^{BIM}	0.0065	0.0130	0.0195	0.0250	0.0306	0.0360	0.0396	0.0450	0.0476	0.0490

and SD denote the 3D boundary element method, Stone and Leal's boundary integral method, and small deformation theory, respectively. By comparing the BEM results and BIM results, we obtain an average percent error (APE) of 1.34% in D_o and 1.16% in D_i, which presents excellent agreement. The APE is calculated by equation 28, where $n = 10$ in this case.

$$APE = \frac{\sum_{k=1}^{n}(|D_{BEM,k} - D_{BIM,k}|/D_{BIM,k})}{n} \times 100\% \qquad (28)$$

In Fig. 5b, we compare the steady state deformation results of compound droplets in a 3D biaxial extensional flow with those by Stone and Leal. In this case, the undisturbed flow is $\boldsymbol{u}^{\infty} = G(x/2, y/2, 2z)$. The constant parameters are $\lambda_o = \lambda_i = 1$, $\Gamma = 0.1$, and $k = 0.5$. The inner capillary number is $5Ca_o$. We calculate the steady state deformation for five out capillary numbers $Ca_o = 0.005$, 0.010, 0.015, 0.020, and 0.025. Good agreement has also been found. In Table 2, we tabulate the steady state deformation in a 3D biaxial flow. Between the results from BEM and BIM, the APE in D_o and D_i is 3.76% and 3.87%, respectively. The APE is also calculated by Eq. 28, while $n = 5$ in this case.
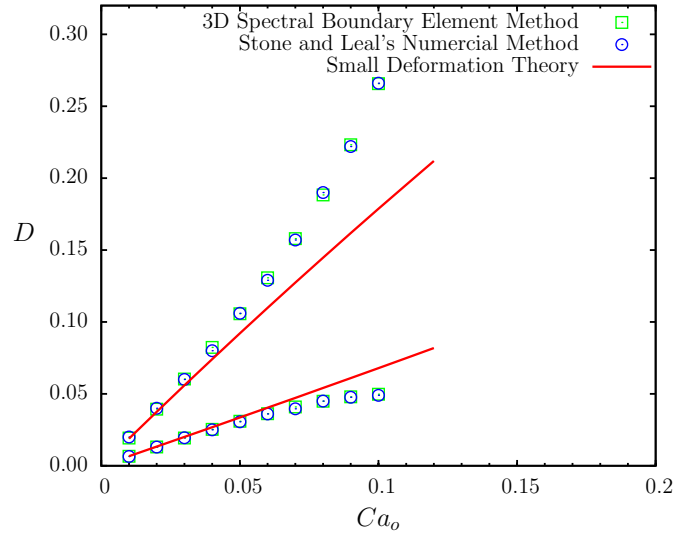
(a) 3D uniaxial flow
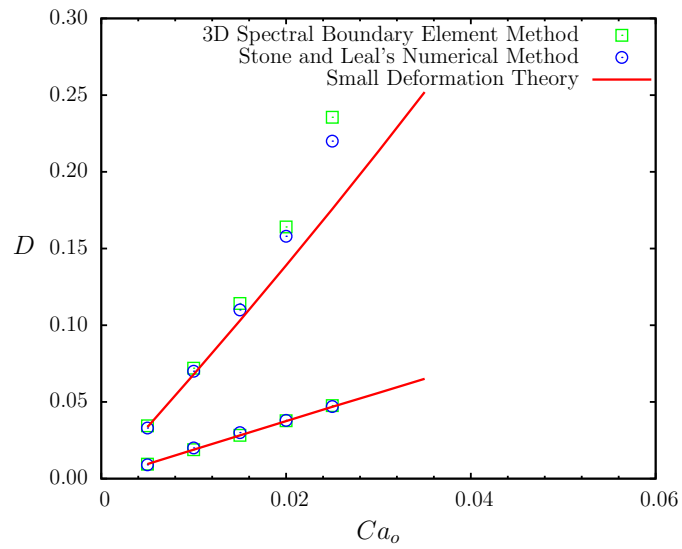
(b) 3D biaxial flow

Figure 5: Comparison of our results with Stone and Leal's in a 3D uniaxial flow and 3D biaxial flow. The square symbols represent the results generated by spectral boundary element method. The round symbols represent Stone and Leal's numerical results. The solid lines are the predictions using small deformation theory. (a) 3D uniaxial flow; (b) 3D biaxial flow.

Table 2: Comparison of steady state deformation generated by Small Deformation Theory (SD), Boundary Element Method (BEM), and Boundary Integral Method (BIM) in a 3D biaxial flow.

Ca_o	0.005	0.010	0.015	0.020	0.025
D_o^{SD}	0.0095	0.0189	0.0282	0.0375	0.0468
D_o^{BEM}	0.0095	0.0189	0.0283	0.0377	0.0476
D_o^{BIM}	0.009	0.020	0.030	0.038	0.047
D_i^{SD}	0.0336	0.0679	0.1030	0.1390	0.1757
D_i^{BEM}	0.0344	0.0720	0.1142	0.1641	0.2356
D_i^{BIM}	0.035	0.070	0.110	0.158	0.220

CHAPTER 4. CONCENTRIC COMPOUND DROPLETS IN A 2D EXTENSIONAL FLOW

In this chapter, we investigated concentric compound droplets that the centroid of the inner droplet coincides with that of the outer droplet. The concentric compound droplets are suspended in a 2D extensional flow, where the undisturbed flow is expressed by $\boldsymbol{u}^\infty = G(x, -y, 0)$. The droplet centroids are placed at the stagnant point of the flow. Under the influence of the 2D extensional flow, the outer droplet deforms into a prolate spherical shape with its longest axis along x axis and its shortest axis along y axis. The steady flow generated inside the outer droplet behaves in the opposite direction to the 2D extensional flow. Therefore, the inner droplet deforms into a prolate spherical shape with its longest axis along y axis and its shortest axis along x axis.

4.1. Influence of the inner droplet size

In this section, we first investigate the influence of the inner droplet size on the deformation and stability of concentric compound droplets. The inner droplet size is represented by a nondimensional parameter size ratio k that is the ratio of a_i to a_o, where a_i and a_o are the radius of the undeformed inner and outer droplets, respectively. In Fig. 6, we plot the transient deformation of a concentric compound droplet for five size ratios $k = 0.40$, 0.65, 0.70, 0.71, and 0.72. The other parameters are constant: $Ca_o = 0.01$, $\Gamma = 0.7$, and $\lambda_o = \lambda_i = 0.2$. As we increase the inner droplet size, the deformation of the outer droplet significantly increases. When k increases from 0.40 to 0.70, the deformation of the outer droplet approximately increases by 180%. Therefore, the existence of the inner droplet has substantial influence on the deformation and stability of the compound droplets, and its influence highly depends on the inner droplet size.

This phenomenon is in agreement with the observation of Davis and Brenner [10], and Stone and Leal [40]. Davis and Brenner studied behavior of an emulsion that contained a solid globe, when the emulsion underwent deformation in a shear flow. They discovered that as they increased the size of the solid globe, the emulsion's deformation increased. Stone and Leal investigated compound droplets deforming induced by a 3D uniaxial extensional flow. They also found out that increasing the inner droplets size could significantly increased the deformation of the outer droplet.

From Fig. 6, we also observe that the compound droplet first deforms rapidly, and most part of the deformation happens in a short time. Then, the deformation gradually slows down and stops, which indicates the compound droplet achieves the steady state. The compound droplet that contains a larger inner droplet needs more time to achieve the steady state. However, when a compound droplet contains a even larger inner droplet, it can no longer reach the steady state and finally breaks up. We define the critical size ratio (k_c) as the maximum size ratio that a compound droplet can reach the steady state. Thus, in the case presented in Fig. 6, the critical size ratio is 0.70. The critical size ratio is useful to decide the maximum volume of the materials that the outer droplet can contain under certain fluids' properties and flow conditions.

Since the capillary number represents the competition between the viscous forces and the surface tension, a droplet with larger capillary number is more deformable. Therefore, we can anticipate that the critical size ratio will decrease as outer capillary number increases. We increase the outer capillary to $Ca_o = 0.1$ and conduct a series of simulation for five size ratios $k = 0.1$, 0.3, 0.41, 0.42, and 0.5. The other parameters are constant, which are $\Gamma = 0.7$ and $\lambda_o = \lambda_i = 0.2$. In Fig. 7, we plot the deformation of both droplets as a function of time for different size ratios. Compared with $Ca_o = 0.01$, compound droplets require more time to achieve a steady state, and

Table 3: Critical size ratio at different outer capillary numbers for $\Gamma = 0.7$ and $\lambda_o = \lambda_i = 0.2$.

Ca_o	0.01	0.03	0.05	0.07	0.10
k_c	0.70	0.59	0.52	0.47	0.41

the critical size ratio reduces to 0.41 when the outer capillary number is $Ca_o = 0.10$. By changing the outer capillary number, we can obtain a series of critical size ratios. As shown in Fig. 8, we plot the critical size ratio (k_c) as a function of outer capillary number (Ca_o). The critical size ratio is inversely proportional to the outer capillary number. Stable compound droplets exist below or on the curve. In Table 3, we list k_c at different Ca_o for $\Gamma = 0.7$ and $\lambda_o = \lambda_i = 0.2$.

To better understand the way in which compound droplets deform as time progresses, we draw the 3D shapes of the outer and inner droplets at different time steps for the case of $Ca_o = 0.10$, $k = 0.4$, $\Gamma = 0.7$, and $\lambda_o = \lambda_i = 0.2$ (Fig. 9). As time progresses, the outer droplet deforms into a prolate spherical shape elongated along x axis, while the inner droplet deforms into a prolate spherical shape elongated along y axis.

To figure out the mechanism of breakup of a compound droplet, we introduce the minimum distance (d_{min}) between the outer interface and the inner interface. This parameter is used to determine whether the breakup is due to the contact of the two interfaces or the continuous extension of a compound droplet [40]. If d_{min} reduces to zero when a compound droplet breaks up, then the breakup is due to the contact of the two interface. In Fig. 10, we plot the curves of d_{min} as a function of time: Fig. 10a is for the case $Ca_o = 0.01$, $\Gamma = 0.7$, $\lambda_o = \lambda_i = 0.2$, and $k = 0.40$, 0.65, 0.70, 0.71, and 0.72, while Fig. 10b is for the case $Ca_o = 0.10$, $\Gamma = 0.7$, $\lambda_o = \lambda_i = 0.2$, and $k = 0.10$, 0.30, 0.41, 0.42, and 0.50. Mainly influenced by the deformation, d_{min} decreases dramatically as the deformation increases and becomes

24
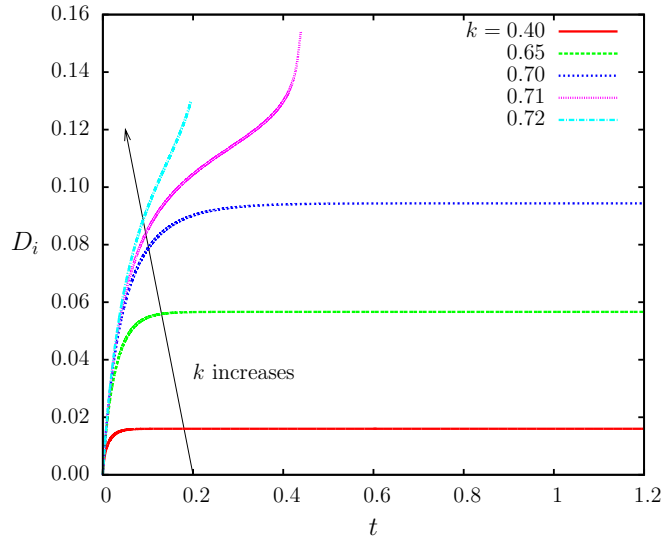
(a) inner
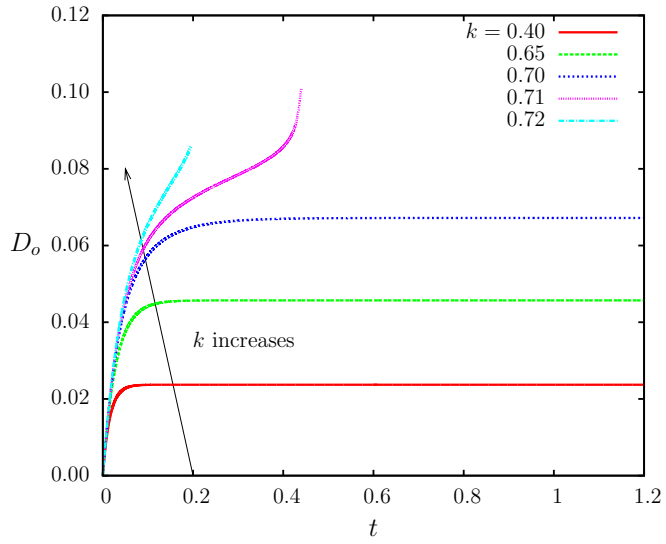
(b) outer

Figure 6: Deformation of the compound droplets as a function of time for different size ratios. The droplets are freely suspended in a 2D extensional flow. $Ca_o = 0.01$, $\Gamma = 0.7$, and $\lambda_o = \lambda_i = 0.2$. The tested size ratios are $k = 0.40$, 0.65, 0.70, 0.71, and 0.72. The critical size ratio is $k_c = 0.70$. (a) Inner droplet deformation D_i vs t. (b) Outer droplet deformation D_o vs t.
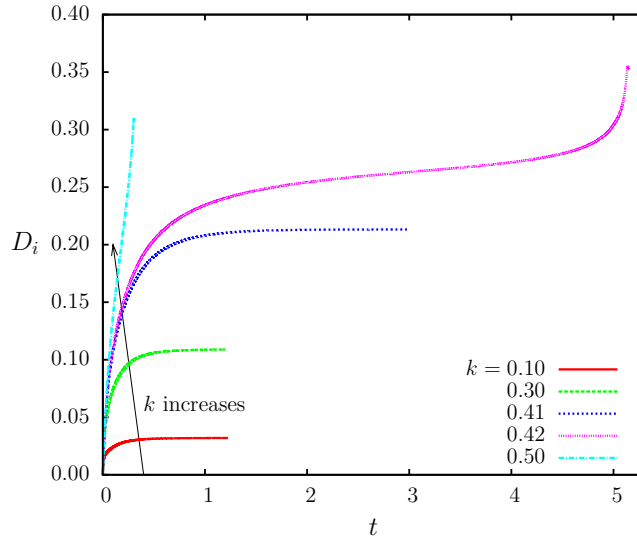
(a) inner
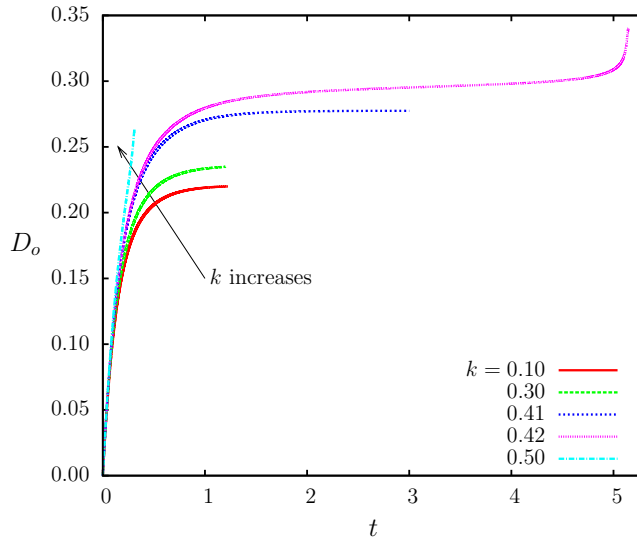
(b) outer

Figure 7: Deformation of the compound droplets as a function of time for different size ratios. The droplets are freely suspended in a 2D extensional flow. $Ca_o = 0.10$, $\Gamma = 0.7$, and $\lambda_o = \lambda_i = 0.2$. The tested size ratios are $k = 0.10$, 0.30, 0.41, 0.42, and 0.50. The critical size ratio is $k_c = 0.41$. (a) Inner droplet deformation D_i vs t. (b) Outer droplet deformation D_o vs t.
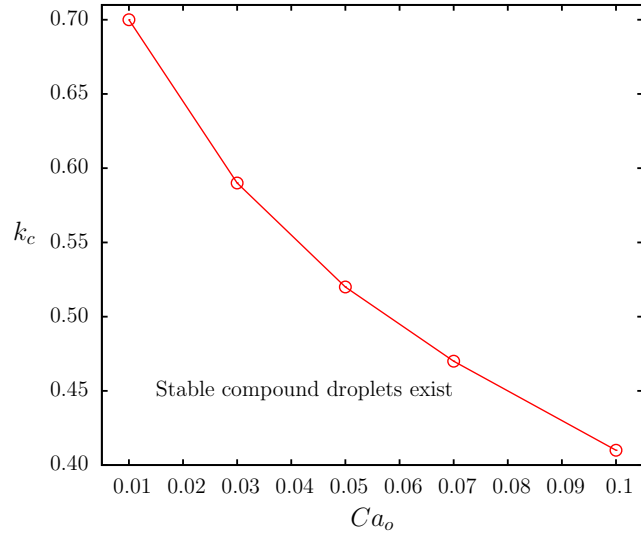
Figure 8: Critical size ratio as a function of the outer capillary number for $\Gamma = 0.7$ and $\lambda_o = \lambda_i = 0.2$. Stable compound droplets exist below the curve.

(a) $t = 0$ (b) 0.1   (c) 0.5   (d) 1   (e) 2

(f) $t = 0$ (g) 0.1   (h) 0.5   (i) 1   (j) 2
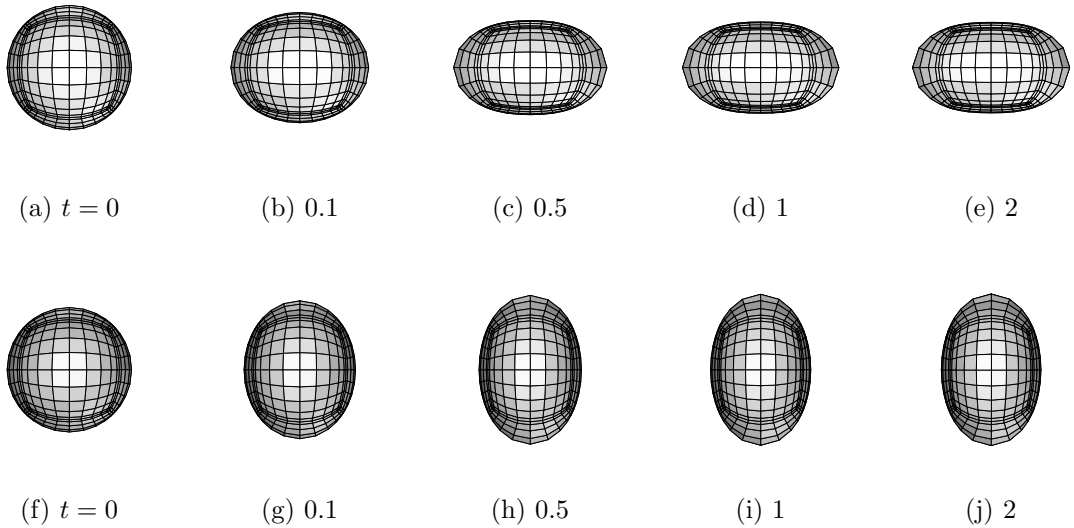
Figure 9: 3D shapes of compound droplets at different time steps for the case of $Ca_o = 0.10$, $k = 0.40$, $\Gamma = 0.7$, and $\lambda_o = \lambda_i = 0.2$. $t = 0$, 0.1, 0.5, 1, and 2. 3D shapes for the outer droplet are from a to e. 3D shapes for the inner droplet are from f to j.

a constant when the deformation stops. When compound droplets are unstable, d_{min} drops to 0, which indicates the breakup of the compound droplet is incurred by the contact of the two interfaces. After the contact of the two interfaces, the inner droplet may continue deform and break through the outer droplet, or it will coalesce with the outer droplet [29, 40], which both lead to the release of the inner material. At this moment, the compound droplet loses its function.

In Fig. 11, we present the time evolution of a compound droplet profiles for an unstable case ($Ca_o = 0.10$, $\Gamma = 0.7$, $\lambda_o = \lambda_i = 0.2$, and $k = 0.42$). As time progresses, the outer droplet and inner droplet elongate along x and y axis, respectively. The inner droplet elongates towards the waist of the outer droplet, which causes d_{min} to decrease. The waists of both droplets shrink because of the conservation of volume. Between $t = 4.5$ and 4.9, the compound droplets are very close to steady state since the profiles are nearly overlapped. However, due to the strong hydrodynamic interaction between the two interfaces, the inner droplet starts deforming again, and the outer droplet subsides at the point closest to the end of the inner droplet. This leads to a rapid increase of the deformation and decrease of d_{min}. Finally, the two interfaces contact each other, and the compound droplets break up. The appearance of a quasi steady state does not occur for cases with parameters far from the critical values. For example, for the compound droplet with parameters of $Ca_o = 0.10$, $\Gamma = 0.7$, $k = 0.50$, and $\lambda_o = \lambda_i$, no quasi steady state exists, and the compound droplet breaks up instantly.

Finally, we address the influence of a small inner droplet on the behavior of the outer droplet. we compute for a compound droplet with $k = 0.1$, 0.2, 0.3, and 0.4. Five outer capillary numbers $Ca_o = 0.01$, 0.03, 0.05, 0.07, 0.10 are considered. The other parameters are fixed: $\Gamma = 0.7$, and $\lambda_o = \lambda_i = 0.2$. Meanwhile, We simulate the behavior of a single droplet for the same outer capillary numbers, while the viscosity

28
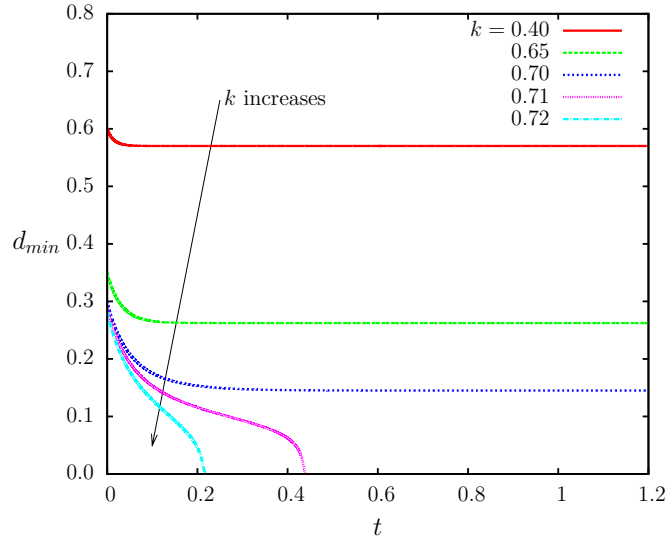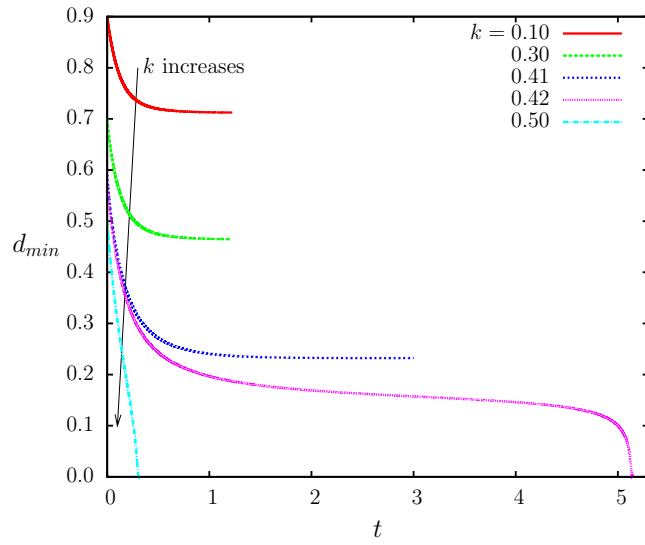
(a) $Ca_o = 0.01$

(b) $Ca_o = 0.10$

Figure 10: The minimum distance between the outer and the inner interface as a function of the time for different size ratios. (a) $Ca_o = 0.01$, $\Gamma = 0.7$, $\lambda_o = \lambda_i = 0.2$, and $k = 0.40$, 0.65, 0.70, 0.71, and 0.72. (b) $Ca_o = 0.10$, $\Gamma = 0.7$, $\lambda_o = \lambda_i = 0.2$, and $k = 0.10$, 0.30, 0.41, 0.42, and 0.50.
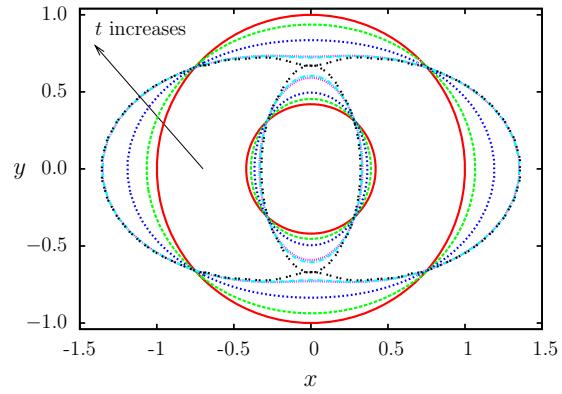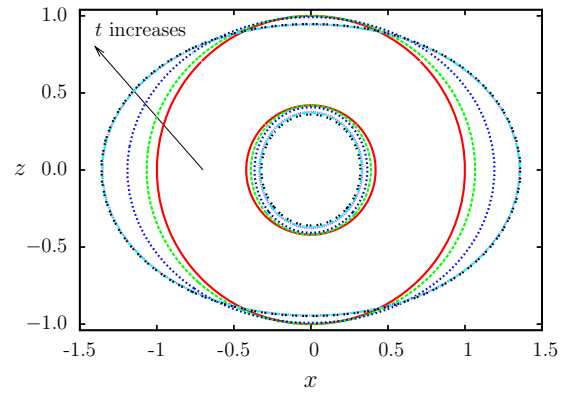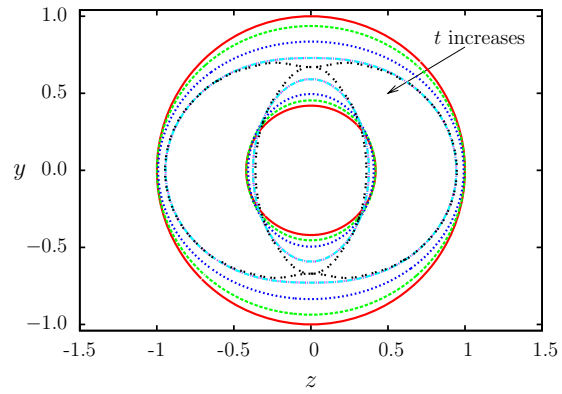
Figure 11: Time evolution of compound droplets profiles for $Ca_o = 0.10$, $\Gamma = 0.7$, $\lambda_o = \lambda_i = 0.2$, and $k = 0.42$. $t = 0$, 0.05, 0.2, 4.5, 4.9, and 5.15. (a) xy plane; (b) xz plane; (c) zy plane.

30

Table 4: Steady state deformation of outer droplets and single droplets and ARD for different size ratios.

Ca_o	0.01	0.03	0.05	0.07	0.10	ARD
$Single$	0.02064	0.06219	0.10462	0.14867	0.22023	
$k = 0.1$	0.02068	0.06232	0.10484	0.14899	0.22071	0.21%
$k = 0.2$	0.02098	0.06323	0.10641	0.15132	0.22451	1.75%
$k = 0.3$	0.02183	0.06584	0.11096	0.15813	0.23606	6.25%
$k = 0.4$	0.02371	0.07168	0.12141	0.17460	0.26942	17.19%

ratio of the droplet to the suspending fluid is 0.2. We compare the steady state deformation of the outer droplet with that of the single droplet in Fig. 12. The solid line with dots represents the deformation of the single droplet. The symbols represent the deformation of the outer droplet for different size ratios k. When $k = 0.1$, the steady state deformation of the outer droplets and that of the single droplets are similar with the average relative difference (ARD) to be approximately 0.21%, which is calculated by

$$ARD = \frac{\sum\limits_{k=1}^{5}(|D_{o,k} - D_{s,k}|/D_{s,k})}{5} \times 100\%, \tag{29}$$

where D_o represents the steady state deformation of the outer droplet, and D_s represents the steady state deformation of the single droplet. In Table 4, we tabulate the steady state deformation of the outer droplet and the single droplet, as well as the ARD for different size ratios. We can observe a remarkable increase of the ARD as the size ratio increases, which demonstrates that the effect of the inner droplet on the deformation of the outer droplet is dependent on the size ratio. When k is smaller than 0.2, the effect of the inner droplet on the outer droplet can be considered as insignificant. From Fig. 12, we can also observe the deformation difference between an outer droplet and a single droplet increases as the outer capillary number increases. Hence, the effect of the inner droplet on the deformation of the outer droplet is also dependent on the outer capillary number. In Fig. 13, we compare the transient
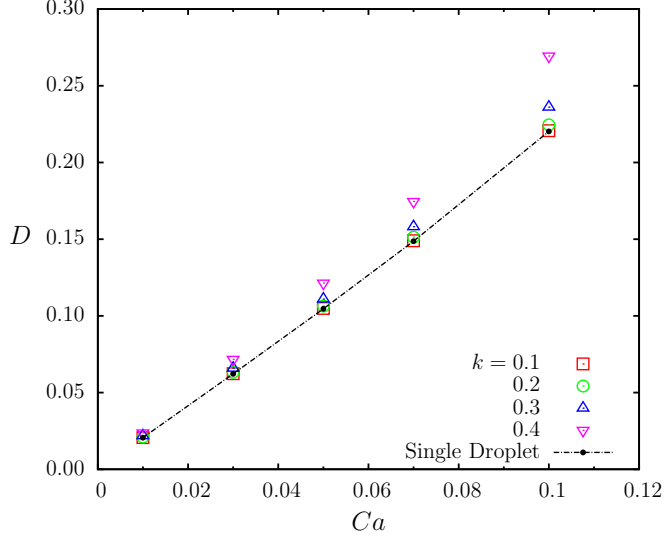
Figure 12: Comparison of the deformation of outer droplets with that of single droplets. Compound droplets have the parameters of $k = 0.1, 0.2, 0.3, 0.4$, $\Gamma = 0.7$, $\lambda_o = \lambda_i = 0.2$, and $Ca_o = 0.01, 0.03, 0.05, 0.07$, and 0.10. Single droplets have the parameters of $\lambda = 0.2$, and $Ca = 0.01, 0.03, 0.05, 0.07$, and 0.10. The solid line with dots represents the deformation of the single droplet, and the solid dots are the single droplets deformation at each capillary. The symbols respent the outer deformation for different size ratios.

deformation of the outer droplets that contain a small inner droplet of $k = 0.1$ with that of the single droplet for $Ca_o = 0.01$ and 0.10. The curves represent the transient deformation of the outer droplet, and the symbols represent the transient deformation of the single droplet. The transient behavior of the outer droplet is also close to the single droplet, which indicates that when the inner droplet is sufficiently small, its influence on the transient behavior of the outer droplet is also negligible.

4.2. Influence of the surface tension ratio

In this section, we address the influence of the material properties on the behavior of compound droplets by changing the surface tension ratio (Γ). The surface tension ratio is defined as the ratio of the inner surface tension to the outer surface

32
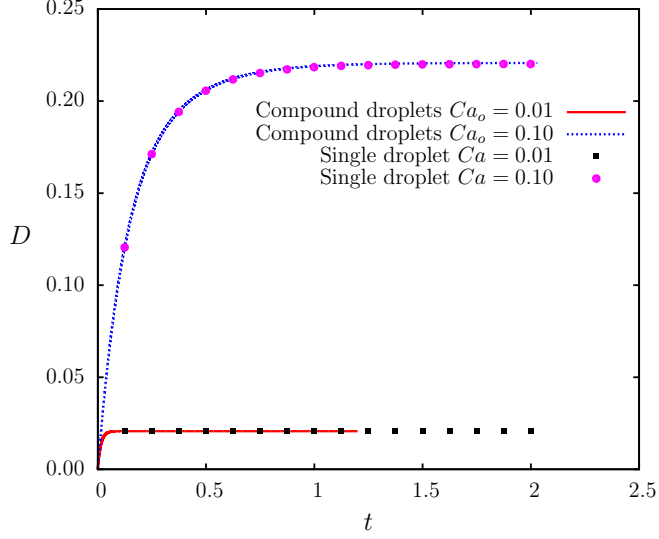
Figure 13: Comparison of the transient deformation of outer droplets with that of single droplets. The lines represent the transient deformation of outer droplets for $k = 0.1$, $\Gamma = 0.7$, and $\lambda_o = \lambda_i = 0.2$, while $Ca_o = 0.01$ and 0.10. The symbols represent the transient deformation of single droplets for $\lambda = 0.2$, while $Ca = 0.01$ and 0.10.

tension. The surface tensions can be calculated by transforming Eqs. 8 and 9 into

$$\gamma_o = \frac{\mu G a_o}{Ca_o}, \tag{30}$$

$$\gamma_i = \frac{\lambda_o \mu G a_i}{Ca_i}. \tag{31}$$

Divide Eq. 31 by Eq 30, the surface tension ratio can be related with another four nondimensionalized parameters, which are size ratios, outer viscosity ratios, outer capillary number, and inner capillary number, in Eq. 32.

$$\Gamma = \frac{Ca_o \lambda_o k}{Ca_i}. \tag{32}$$

Since the outer capillary number, outer viscosity ratio, and size ratio are constant in Eq. 32, only the inner capillary is varying with the surface tension ratio, and

33

it is in inverse proportion to the surface tension ratio. As the inner capillary number determines the deformability of the inner droplet, the inner droplet is less deformable given a higher surface tension ratio.

We conduct a series of simulation for the compound droplets with five different surface tension ratios $\Gamma = 0.40$, 0.08, 0.05, 0.04, and 0.03. The other parameters are constant ($Ca_o = 0.01$, $k = 0.4$, and $\lambda_o = \lambda_i = 0.2$). In Fig. 14, we plot the deformation of both inner and outer droplets as a function of time. As Γ decreases, the deformation of both the inner and outer droplets increases. The influence of Γ is more significant for the deformation of the inner droplet. For example, the steady state deformation of the inner droplet is 0.0280 when $\Gamma = 0.4$ and 0.3556 when $\Gamma = 0.05$, the latter is 12.7 times of the former; while, at the same time, the steady state deformation only increases by 10% for the outer droplet. As Γ decreases, a compound droplet needs more and more time to achieve steady state. When $\Gamma = 0.04$, the compound droplet cannot reach steady state and eventually breaks up. We define the critical surface tension ratio (Γ_c) as the minimum surface tension ratio that a compound droplet can reach steady state. Thus, in the case presented in Fig. 14, the critical surface tension ratio is $\Gamma_c = 0.05$. The critical surface tension ratio is useful for determining the material properties of a stable compound droplet.

We also carry out a series of simulation to find the critical surface tension ratios for outer capillary numbers of $Ca = 0.03$, 0.05, 0.07, and 0.10, while the other parameters are constant $k = 0.4$, and $\lambda_o = \lambda_i = 0.2$. In Fig. 15, we plot the critical surface tension ratio as a function of the outer capillary number. As the outer capillary number increases, the critical surface tension ratio also increases. Stable compound droplets exist above and on the curve. In Table 5, we list the critical surface tension ratio at different outer capillary numbers for $k = 0.4$ and $\lambda_o = \lambda_i = 0.2$.

To examine the breakup mechanism, we plot d_{min} as a function of the time
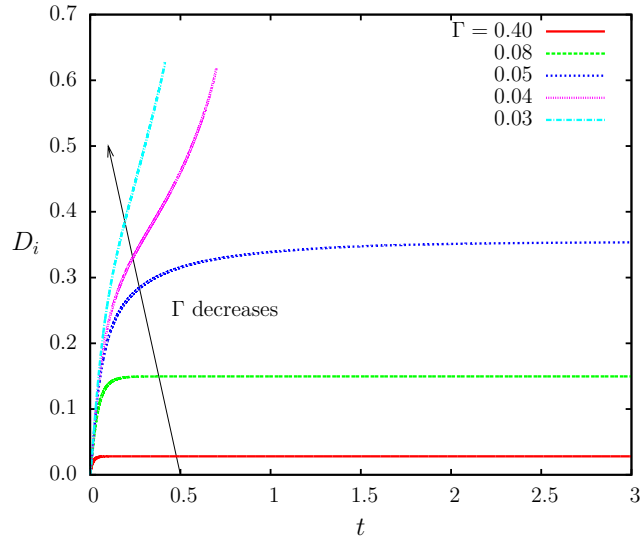
(a) inner
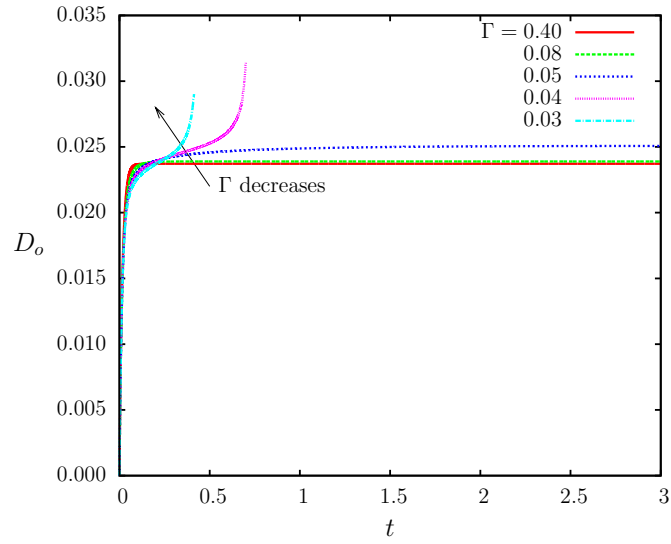
(b) outer

Figure 14: The deformation of compound droplets as a function of time for different surface tension ratios. The compound droplets are suspended in a 2D extensional flow. $Ca_o = 0.01$, $k = 0.40$, and $\lambda_o = \lambda_i = 0.2$. The tested surface tension ratios are $\Gamma = 0.40$, 0.08, 0.05, 0.04, and 0.03. The critical surface tension ratio is $\Gamma_c = 0.05$. (a) Inner droplet deformation D_i vs t. (b) Outer droplet deformation D_o vs t.
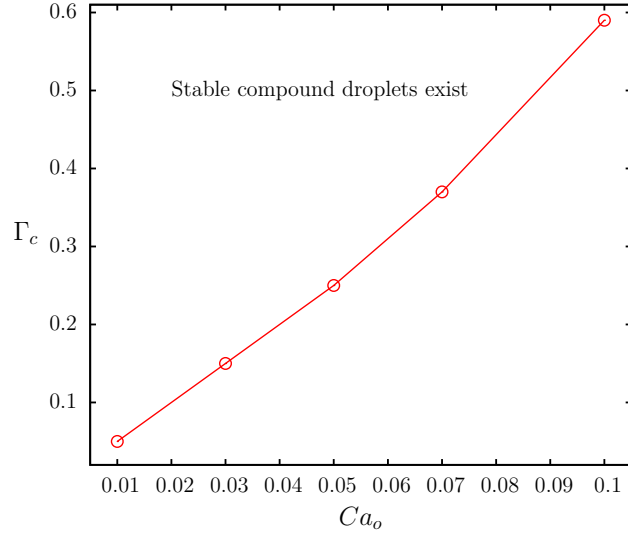
Figure 15: Critical surface tension as a function of the outer capillary number for $k = 0.40$ and $\lambda_o = \lambda_i = 0.2$. Stable compound droplets exist above the curve.

Table 5: Critical surface tension ratio at different outer capillary numbers for $k = 0.40$ and $\lambda_o = \lambda_i = 0.2$.

Ca_o	0.01	0.03	0.05	0.07	0.10
Γ_c	0.05	0.15	0.25	0.37	0.59

for $Ca_o = 0.01$ and $Ca_o = 0.10$ (Fig. 16). As the surface tension ratio decreases, the minimum distance between the two interfaces also decreases at the time that a compound droplet achieves steady state. This is because as Γ decreases, the inner capillary increases and the inner droplet becomes more deformable. When compound droplets break up, the minimum distance between the two interfaces suddenly decreases. In Fig. 17, we present the time evolution of the compound droplets profiles for $Ca_o = 0.01$, $\Gamma = 0.03$, $\lambda_o = \lambda_i = 0.2$, and $k = 0.4$. As the time progresses, the outer droplet only deforms slightly due to the small outer capillary number, while the inner droplet elongates dramatically and eventually breaks up. Therefore, the breakup mechanism in this situation is the continuous extension of the inner droplet. It is not surprising that when the outer droplet is nearly undeformable, the inner droplet can continuously deform until break up before it contacts the outer droplet.

4.3. Influence of the viscosity ratios

4.3.1. Influence on the deformation of compound droplets

Firstly, we investigate the influence of outer viscosity ratio λ_o (the viscosity ratio of Fluid 2 to Fluid 3) on the behavior of the compound droplets. We examine the behavior of compound droplets for nine outer viscosity ratios $\lambda_o = 2 \times 10^{-4}$, 2×10^{-3}, 2×10^{-2}, 0.2, 1, 5, 10, 50, and 100. The other parameters are constant: $Ca_o = 0.05$, $k = 0.5$, $\Gamma = 0.7$, and $\lambda_i = 1$. In Fig. 18, we plot the steady state deformation as a function of the outer viscosity ratio. The open circle and filled circle symbols represent the deformation of the outer droplet and inner droplet, respectively. The behavior of the deformation is not monotonous and has three stages. When the outer viscosity is sufficiently small, e.g. from 2×10^{-4} to 2×10^{-2}, the deformation of the outer droplet is nearly constant; the deformation of the inner droplet is close to 0 because the viscous force on the inner droplet is negligible compared to the surface
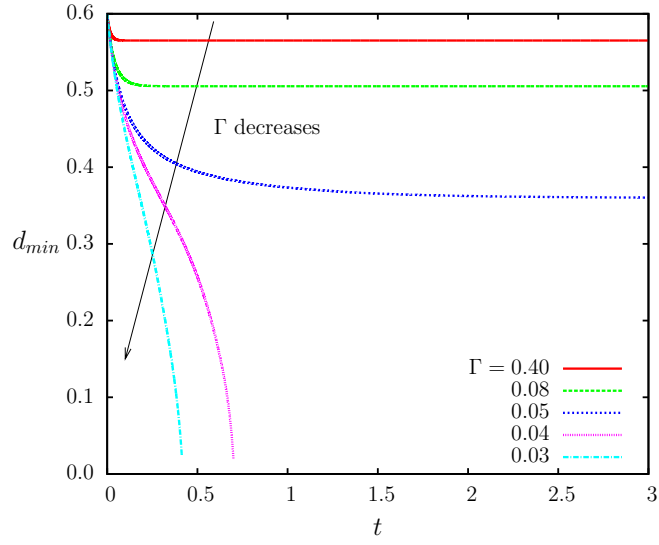
(a) $Ca_o = 0.01$
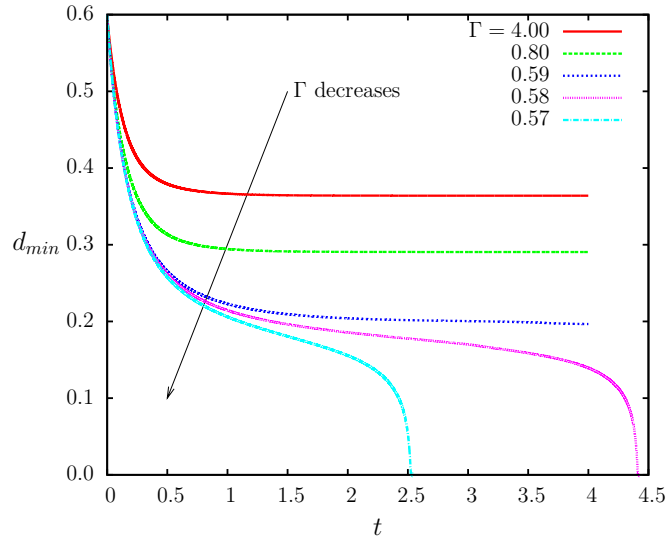
(b) $Ca_o = 0.10$

Figure 16: The minimum distance between the outer and inner interface as a function of the time for different surface tension ratios. (a) $Ca_o = 0.01$, $k = 0.4$, $\lambda_o = \lambda_i = 0.2$, and $\Gamma = 0.40$, 0.08, 0.05, 0.04, and 0.03. (b) $Ca_o = 0.10$, $k = 0.4$, $\lambda_o = \lambda_i = 0.2$, and $\Gamma = 4.00$, 0.80, 0.59, 0.58, and 0.57.

38
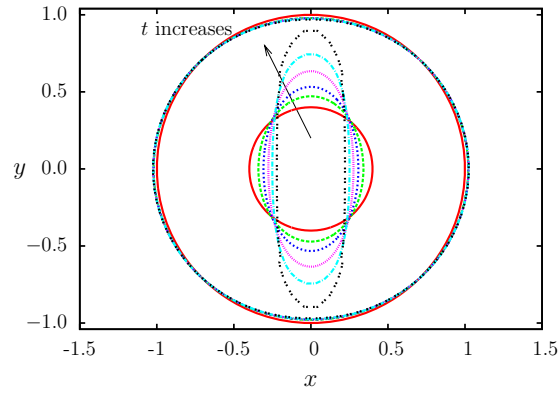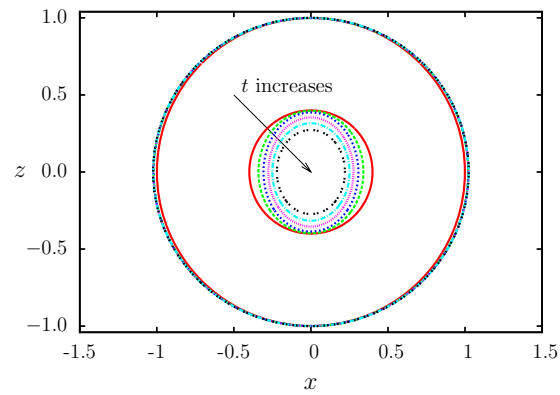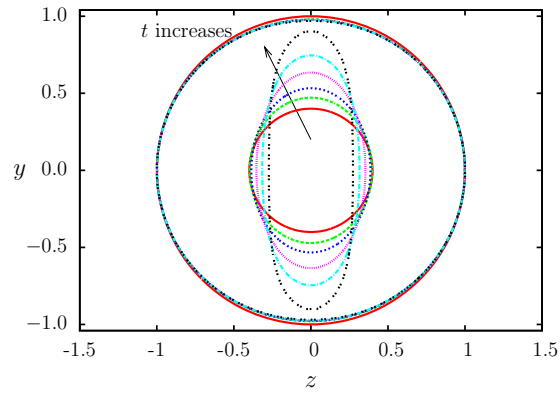
Figure 17: Time evolution of compound droplets profiles for $Ca_o = 0.01$, $\Gamma = 0.03$, $\lambda_o = \lambda_i = 0.2$, and $k = 0.40$. $t = 0$, 0.05, 0.1, 0.2, 0.3, and 0.4. (a) xy plane; (b) xz plane; (c) zy plane.

39
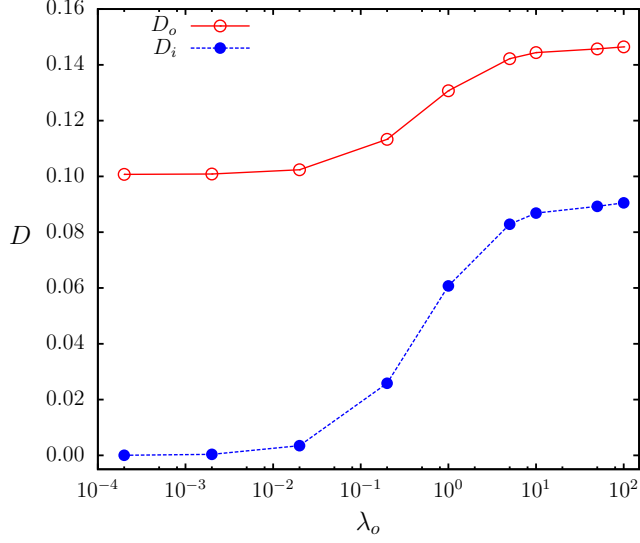
Figure 18: Steady state deformation of compound droplets as a function of outer viscosity ratio for $Ca_o = 0.05$, $k = 0.50$, $\Gamma = 0.7$, and $\lambda_i = 1$. The outer viscosity ratios examined are $\lambda_o = 2 \times 10^{-4}$, 2×10^{-3}, 2×10^{-2}, 0.2, 1, 5, 10, 50, and 100. The empty circle symbols are outer deformation. The solid circle symbols are inner deformation.

tension ($Ca_i = \frac{\lambda_o \mu Ga_i}{\gamma_i} = O(0)$, when $\lambda_o = O(0)$). As λ_o increases in the range of 2×10^{-2} to 5, the deformation of both inner and outer droplet increases, and the deformation of the inner droplet grows faster and dramatically. The deformation of the inner droplet is more sensitive to the outer viscosity ratio because the inner capillary number is directly proportional to the outer viscosity ratio. When the outer viscosity ratio is greater than 10, droplet deformation is independent on λ_o.

Secondly, we investigate the influence of the inner viscosity ratio λ_i (the viscosity ratio of Fluid 1 to Fluid 3) on the behavior of compound droplets. We study a series of cases with constant parameters of $Ca_o = 0.05$, $k = 0.5$, $\Gamma = 0.7$, and $\lambda_o = 1$, while the inner viscosity ratio is varied $\lambda_i = 2 \times 10^{-4}$, 2×10^{-3}, 2×10^{-2}, 0.1, 0.2, 0.4, 1, and 1.5. In Fig. 19, we plot the steady state deformation of the compound droplets versus the inner viscosity ratio. We can observe that when the inner viscosity ratio
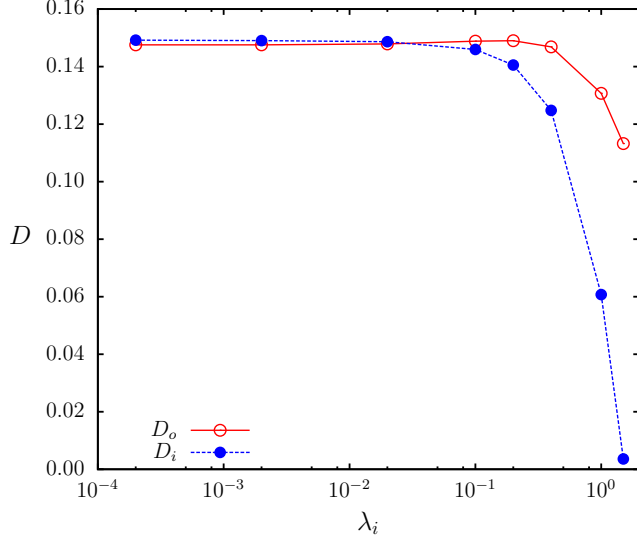
Figure 19: Steady state deformation of compound droplets as a function of inner viscosity ratio. The inner viscosity ratios examined are $\lambda_i = 2 \times 10^{-4}$, 2×10^{-3}, 2×10^2, 0.1, 0.2, 0.4, 1, and 1.5, while the other parameters are constant, $Ca_o = 0.05$, $k = 0.5$, $\Gamma = 0.7$, and $\lambda_o = 1$. The empty circle symbols are outer deformation. The solid circle symbols are inner deformation.

is sufficiently small, e.g. 2×10^{-4} to 2×10^{-2}, the steady state deformation for both droplets keeps nearly constant. This phenomena indicates that when Fluid 2 is more viscous than Fluid 1, the steady state deformation does not change much with the change of the inner viscosity ratio. As the inner viscosity increases in the range of 0.2 to 1.5, the deformation of the compound droplets decreases rapidly. When the inner viscosity is 1.5, the deformation of the inner droplet drops to 0.0036.

Since the breakup of the compound droplets is closely related to the deformation, the viscosity ratios can influence the breakup. In next section, we address this influence.

4.3.2. Influence on the breakup of compound droplets

In order to understand how viscosity ratios influence the breakup of compound droplets, we investigate their effect on the critical size ratio. We first investigate the

inner viscosity ratio. We complete a series of simulation to obtain the critical size ratio, while $Ca_o = 0.1$, $\Gamma = 0.7$, $\lambda_o = 0.2$, and $\lambda_i = 1$. In Fig. 20, we plot d_{min} as a function of time. we observe that the compound droplet break up at $k = 0.64$ because of the contact of the two interfaces. In this case, the critical size ratio is 0.63. As shown in Table 3, the critical size ratio is 0.41 when the parameters for the compound droplets are $Ca_o = 0.1$, $\Gamma = 0.7$, $\lambda_o = 0.2$, and $\lambda_i = 0.2$. The increase of the inner viscosity ratio has greatly increasesd the critical size ratio, which indicates that increasing the inner viscosity ratio will increase the stability of the compound droplet. In Fig. 21, we present the time evolution of the compound droplets profiles on xy plane for $Ca_o = 0.1$, $k = 0.42$, and $\lambda_o = 0.2$, while λ_i is 0.2 and 1, so we can have an insight of how the inner viscosity ratio influences the behavior of the compound droplets. Fig. 21a shows that when $\lambda_i = 0.2$, the compound droplet is unstable. The breakup takes place due to the contact of the two interfaces. Both inner and outer droplets have large deformation. The inner droplet deforms into an olive shape with nearly pointed ends. This behavior is similar to a single droplet that has a low viscosity. The strong hydrodynamic interaction between the two interfaces not only brings two interfaces together, but also causes the outer droplet to subside at the point closest to the end of the inner droplet. As shown in Fig. 21b, when $\lambda_i = 1$, the compound droplet is stable. The inner droplet deforms slightly, and the deformation of outer droplet is also smaller than the outer deformation for $\lambda_i = 0.2$. The increase of the inner viscosity ratio decreases the deformation of the compound droplet, and thus it stabilizes the compound droplet.

As we increase the inner viscosity ratio, the outer viscosity shows different effects on the stability of compound droplet. We first examine compound droplets with an small inner viscosity ratio of $\lambda_i = 0.2$ for three outer viscosity ratios $\lambda_o = 0.02$, 0.2, and 1. The other parameters for the compound droplets are constant $Ca_o = 0.05$,

Figure 20: Minimum distance between two interfaces as a function of the size ratio. $Ca_o = 0.1$, $\Gamma = 0.7$, $\lambda_o = 0.2$, and $\lambda_i = 1$. When $k = 0.64$, the compound droplets break up because of the contact of the two interfaces. The critical size ratio is 0.63.

$\Gamma = 0.7$, and $k = 0.53$. As shown in Fig. 22, when $\lambda_o = 0.02$, the compound droplet is unstable and breaks up instantly; when λ_o increases to 0.2, the compound droplet exists for a longer time although it eventually breaks up; as λ_o increases to 1, the compound droplet is able to achieve steady state. In Fig. 23, we plot the time evolution of the compound droplets profiles for $Ca_o = 0.05$, $k = 0.53$, $\Gamma = 0.7$, while $\lambda_o = 0.2$ and 1. Fig. 23a shows that when $\lambda_o = 0.2$, the inner droplet has very large deformation and deforms into a olive shape, and the outer droplet subsides at its waist. In this case, the compound droplet breaks up because the two interfaces contact each other. As shown in Fig. 23b, when outer viscosity increases to 1, the compound droplet reaches the steady state. The inner droplet deforms more slowly compared to $\lambda_o = 0.2$. When $t = 0.1$, the inner droplet is nearly undeformed for $\lambda_o = 1$, while the inner droplet has already significantly deformed for $\lambda_o = 0.2$.

However, when $\lambda_i = 1$, increasing the outer viscosity ratio will destabilize compound droplets. We seek for the critical size ratio of compound droplets that have

43
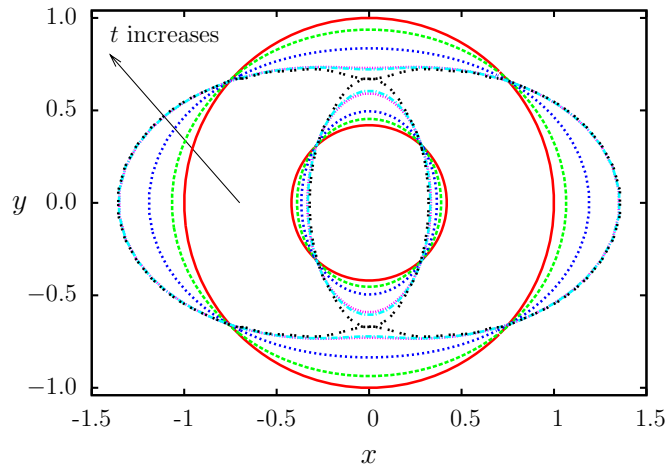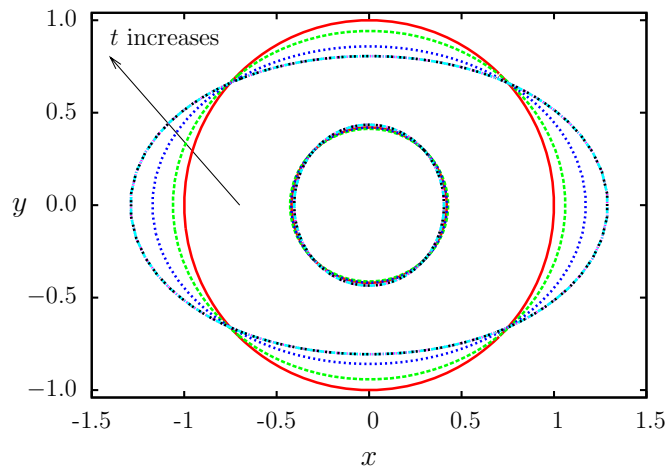
(a) $\lambda_i = 0.2$

(b) $\lambda_i = 1$

Figure 21: Time evolution of the compound droplets profiles for $Ca_o = 0.10$, $k = 0.42$, $\Gamma = 0.7$, and $\lambda_i = 0.2$. (a) $\lambda_i = 0.2$, and $t = 0$, 0.05, 0.2, 4.5, 4.9, and 5.15; (b) $\lambda_i = 1$, and $t = 0$, 0.05, 0.2, 4.5, 4.9, and 5.15.
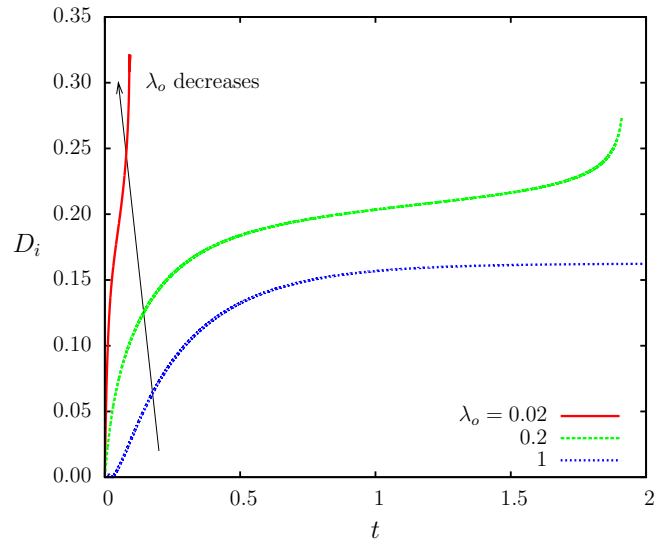
(a) inner
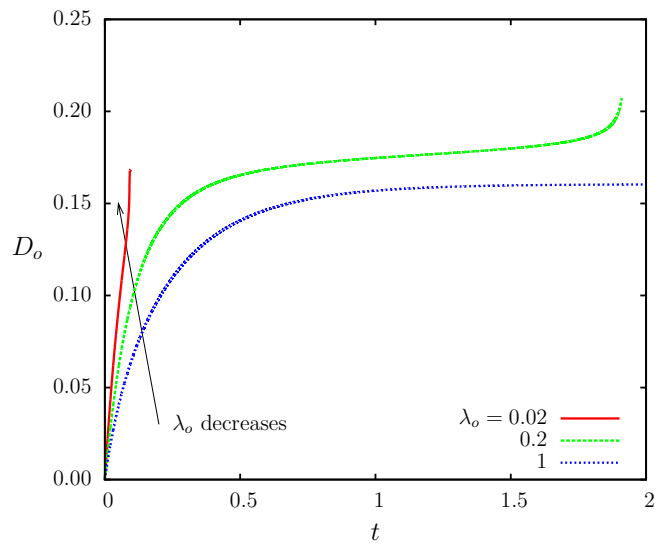
(b) outer

Figure 22: The influence of the outer viscosity ratio on the deformation of the compound droplets. $Ca_o = 0.05$, $k = 0.53$, $\Gamma = 0.7$, $\lambda_i = 0.2$, and $\lambda_o = 0.02$, 0.2, and 1. (a) Inner droplet deformation vs t; (b) Outer droplet deformation vs t.

45
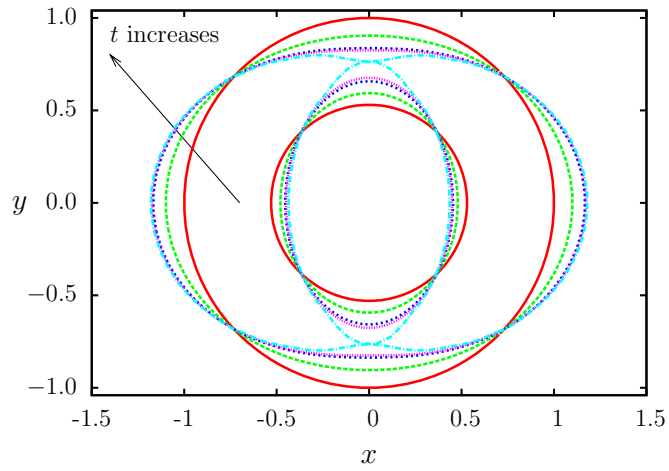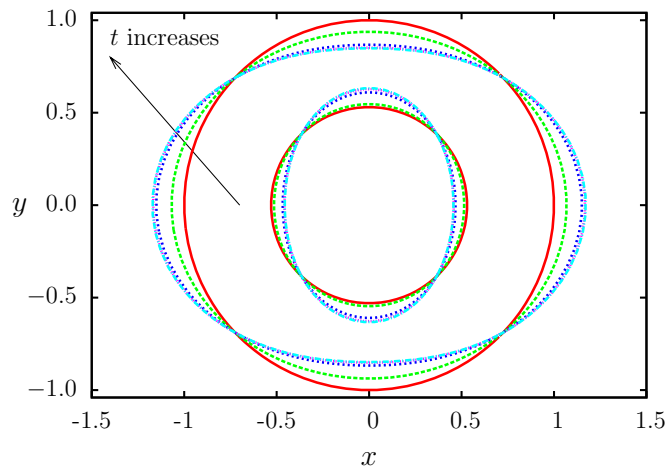
Figure 23: Time evolution of the compound droplets profiles for $Ca_o = 0.05$, $k = 0.53$, $\Gamma = 0.7$, and $\lambda_i = 0.2$. (a) $\lambda_o = 0.2$, and $t = 0$, 0.1, 0.5, 1, and 1.92. (b) $\lambda_o = 1$, and $t = 0$, 0.1, 0.5, 1, and 2.
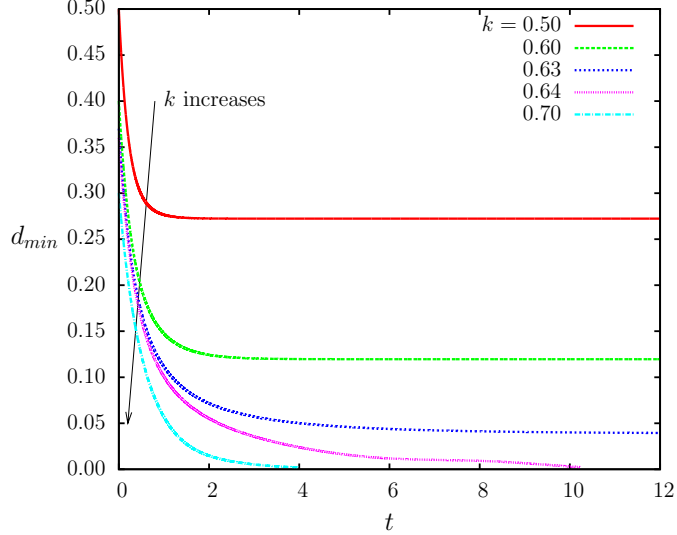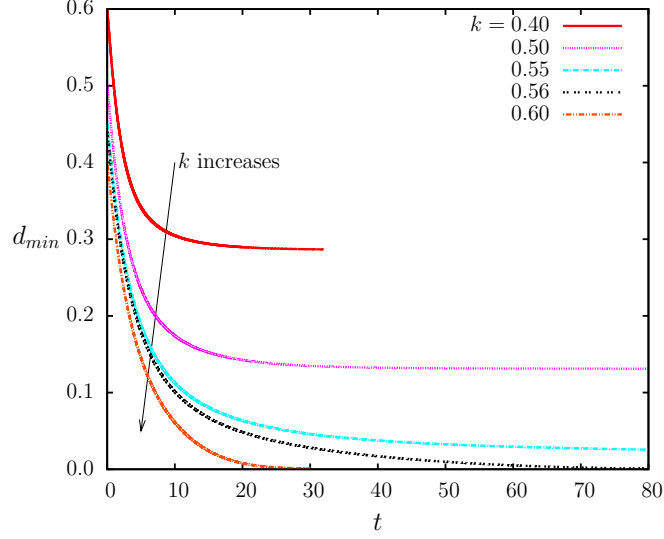
Figure 24: Minimum distance between two interfaces as a function of the size ratio. $Ca_o = 0.1$, $\Gamma = 0.7$, $\lambda_o = 10$, and $\lambda_i = 1$. When $k = 0.56$, the compound droplets break up because of the contact of the two interfaces. The critical size ratio is 0.55.

parameters of $Ca_o = 0.1$, $\Gamma = 0.7$, $\lambda_i = 1$, and $\lambda_o = 10$. As shown in Fig. 24, the compound droplets break up at $k = 0.56$ due to the contact of the two interfaces, and the critical size ratio is 0.55. When $Ca_o = 0.1$, $\Gamma = 0.74$, $\lambda_o = 0.2$, and $\lambda_o = 0.2$, the critical size ratio is 0.63 as depicted in Fig. 20. The increase of the outer viscosity ratio decreases the critical size ratio, thus it decreases the stability of compound droplets. This may be due to the fact that as the outer viscosity increases, the deformation of the compound droplet also increases, and the two interfaces become easier to contact each other. section

4.4. Conclusion of concentric compound droplets

For concentric compound droplets, we investigate the influence of three major parameters on the deformation and stability of the compound droplet. These parameters are size ratio, surface tension ratio, and viscosity ratios.

The presence of the inner droplet substantially influences the deformation and stability of the compound droplet depending on the size of the inner droplet. As we increase the size of the inner droplet, the deformation of both outer and inner droplets increases. This behavior reduces the stability of the compound droplet. With a larger inner droplet and higher deformation, the two interfaces of the compound droplets become easier to contact each other. We investigate the critical size ratio under different outer capillary numbers. The critical size ratio decreases as the outer droplet capillary number increases. However, when the inner droplet is sufficiently small such as $k = 0.1$, its influence on the outer droplet is negligible, and the outer droplet behaves similarly to a single droplet.

The surface tension ratio mainly influences the deformation of the inner droplet. Its influence on the deformation of the outer droplet is limited. As we decreases the surface tension ratio, the deformation of the inner droplet increases dramatically. On one hand, when the outer capillary number is small and the outer droplet is less deformable such as $Ca_o = 0.01$, the inner droplet continues deforming until breaks up without contact the outer interface. On the other hand, when the outer capillary number is larger, the inner deforms until contacts the outer interface and causes the whole compound droplet to break up. We investigate the critical surface tension ratio under different outer capillary numbers. The critical surface tension ratio increases as the outer capillary number increases.

When the inner viscosity ratio (λ_i) is small, it has very little influence on the steady state deformation of both outer and inner droplets. For moderate values of λ_i, the deformation of both droplets decreases rapidly. We investigate the influence of the inner viscosity on the critical size ratio for a compound droplet with constant parameters of $Ca_o = 0.10$, $\Gamma = 0.7$, and $\lambda_o = 0.2$. As the inner viscosity ratio increases from 0.2 to 1, the critical size ratio increases from 0.42 to 0.63. This indicates

that the increase of the inner viscosity ratio stabilizes the compound droplet. When the outer viscosity ratio is small, it also has insignificant influence on the steady state deformation of both outer and inner droplets. Contrary to the effect of the inner viscosity ratio, as the outer viscosity ratio increases, the deformation of both droplets increases dramatically. The deformation of the inner droplet reacts sharply against the change of the outer viscosity ratio because the inner capillary number is directly proportional to the outer viscosity ratio. When the outer viscosity ratio is greater than 10, the steady deformation of both inner and outer droplets stops growing with the increase of the outer viscosity ratio. The value of the outer viscosity has different influence on the stability of the compound droplet within different range of the inner viscosity ratio. When $\lambda_i \ll 1$, the increase of λ_o increases the stability of the compound droplet; when $\lambda_i = O(1)$, the increase of λ_o decreases the stability of the compound droplets.

CHAPTER 5. ECCENTRIC COMPOUND DROPLETS IN A 2D EXTENSIONAL FLOW

Eccentric compound droplets are more complex than concentric compound droplets because their centers of mass are not coincident. The tests for eccentric compound droplets could be countless if we consider every possible initial position of both outer and inner droplet centroid. To simplify the problem, we start computations with the initial outer droplet centroid at the stagnant point of the flow and the initial inner droplet centroid on x, y, or z axis. In this chapter, we investigate the effect of the initial placement of the inner droplet on the behavior of compound droplets.

5.1. Internal droplet on x axis

We investigate eccentric compound droplets with constant parameters of $Ca_o = 0.10$, $k = 0.38$, $\Gamma = 0.5$, and $\lambda_o = \lambda_i = 0.2$. Concentric compound droplets with the same parameters can reach steady state. The centroid of the inner droplet is initially placed on positive x axis, thus its center of mass has the coordinate of $(\delta, 0, 0)$, where δ is the eccentricity that can be calculated using Eq. 7 as mentioned in Section 2.2. We examine four eccentricities 0.1, 0.2, 0.4, and 0.6.

In Fig. 25, we plot the deformation of both droplets as a function of time. For the inner droplets, the deformation curves are overlapped before $t = 3$. During this period, the inner deformation first increases rapidly and then levels off. After $t = 3$, the deformation continues to increase again, and the inner droplet finally breaks up. The compound droplets with larger eccentricity breaks up earlier. However, the eccentricity has insignificant influence on the deformation of the outer droplet. All the deformation curves of the outer droplet overlap each other, although the compound droplet has different eccentricities. These curves are also overlapped with the curve of $\delta = 0$ which is the deformation curve of a concentric compound droplet. In this

case, only the inner droplet breaks up, thus the internal material is not released and the compound droplet is still functional.

In Fig. 26, we investigate the x-component of the centroidal velocity (u_x^c) as a function of time. The centroidal velocity is the velocity of the center of mass. The velocity of the inner droplet is negative, thus the inner droplet is moving in the negative x direction, which indicates the stream along x axis flows to the stagnant point. The absolute value of $u_{x,i}^c$ first increases slightly and then decreases rapidly. It drops to nearly 0 and levels off after $t = 1.5$ and continues increasing after $t = 2.5$. The outer droplet also gains a negative velocity since $t = 0$. The absolute value of the velocity first increases and then decreases, which responds to the motion of the inner droplet. It continues increasing after $t = 1.5$ which is earlier than the inner droplet. We explain the reason that compound droplets continue accelerating after the inner droplet reaches the stagnant point as follows. The 2D extensional flow generates a net force on the outer interface. When the outer droplet is at the stagnant point, this net force is balanced due to the symmetry. As shown in Fig. 27, as the inner droplet moves from the eccentric point to the stagnant point, it slightly accelerates the outer droplet and moves the outer droplet away from the stagnant point, which causes the net force on the outer droplet to lose the balance and start accelerating the outer droplet in the negative x direction. At the same time, the flow inside the outer droplet loses its symmetry and continues to move the inner droplet in the negative x direction. To be mentioned, when we place the inner droplet on x axis, the y and z components of the velocity are always zero, which indicates that the flow field inside the outer droplet is symmetric along y and z axes.

In Fig. 28, we investigate u_x^c as a function of x^c, where x^c is x-component of the position of the droplet centroid. As the inner droplet approaches the stagnant point, the centroidal velocity of the inner droplet decreases rapidly. When the inner
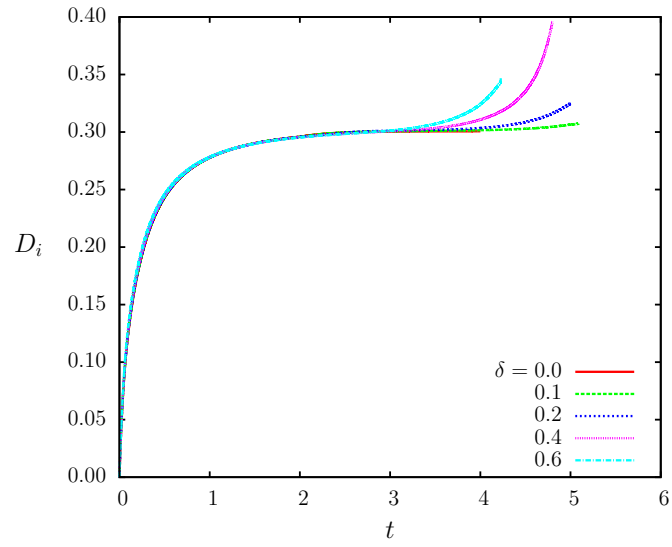
(a) inner
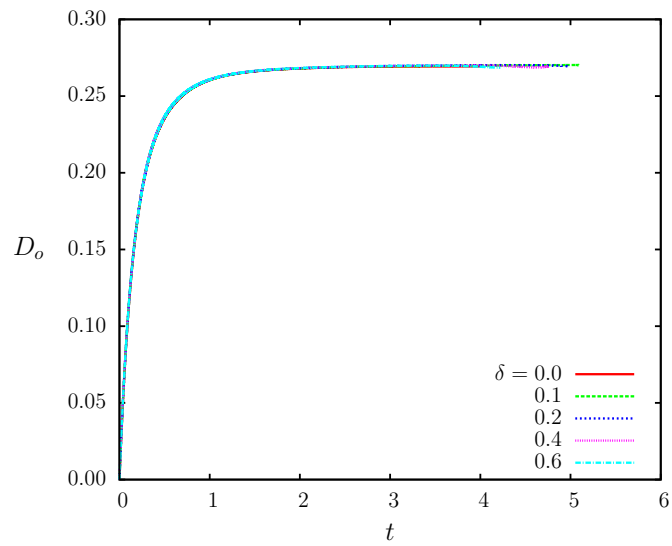
(b) outer

Figure 25: The influence of eccentricity on the deformation of the compound droplet. $Ca_o = 0.10$, $k = 0.38$, $\Gamma = 0.5$, $\lambda_o = \lambda_i = 0.2$, and $\delta = 0$, 0.1, 0.2, 0.4, and 0.6. The inner droplet is on the x axis.

52
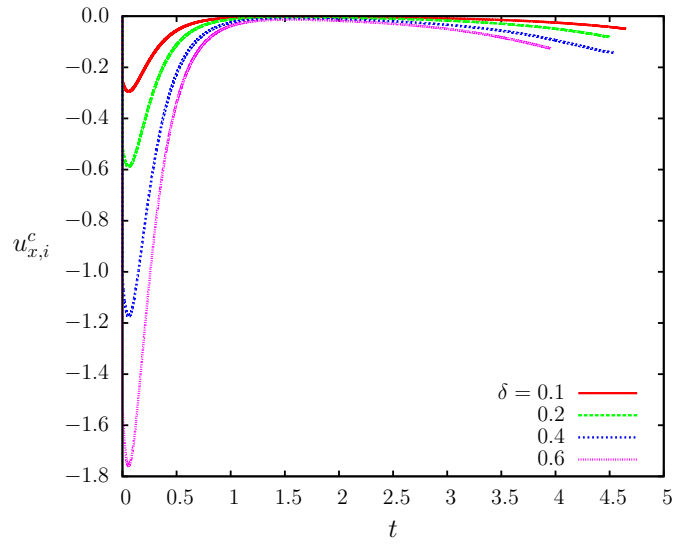
(a) inner
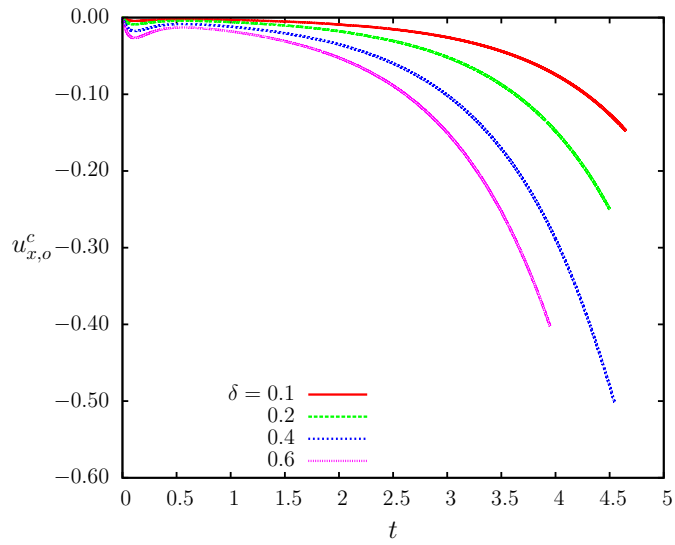
(b) outer

Figure 26: The influence of eccentricity on the x-component of the centroidal velocity for $Ca_o = 0.10$, $k = 0.38$, $\Gamma = 0.5$, $\lambda_o = \lambda_i = 0.2$, and $\delta = 0.1$, 0.2, 0.4, and 0.6.

Figure 27: x_i^c as a function of x_o^c for $Ca_o = 0.10$, $k = 0.38$, $\Gamma = 0.5$, $\lambda_o = \lambda_i = 0.2$, and $\delta = 0.1$, 0.2, 0.4, and 0.6.

droplet reaches the stagnant point, the velocity nearly drops to zero. This implies that the flow field near the stagnant point is very weak. Fig. 28b shows that the velocity curves vary slightly in the range of $x_o^c \in [0, 0.03]$ and completely overlap after $x_o^c = 0.03$. The slight variation of the velocity is caused by the eccentricity. The outer droplet is only dominated by the extensional flow after it leaves the stagnant point.

Fig. 29 presents the time evolution of the compound droplets profiles for $\delta = 0.1$, 0.2, 0.4, and 0.6. The compound droplets deform and migrate at the same time. The outer droplet elongates along the x axis due to the 2D extensional flow. The inner droplet still elongates along the y axis regardless of the eccentricity, and this behavior is the same as the concentric case. The inner droplet quickly moves towards the stagnant point and stalls at the stagnant point. At the same time, the outer droplet still continues moving in the negative x direction slightly, and its centroidal velocity becomes higher and higher, until the compound droplet breaks up.

(a) inner

(b) outer

Figure 28: The x-component of the centroidal velocity as a function of the x-component of the position of the droplet centroid for $Ca_o = 0.10$, $k = 0.38$, $\Gamma = 0.5$, $\lambda_o = \lambda_i = 0.2$, and $\delta = 0.1$, 0.2, 0.4, and 0.6.

Figure 29: Time evolution of compound droplets profiles on xy plane for $Ca_o = 0.10$, $k = 0.38$, $\Gamma = 0.5$, $\lambda_o = \lambda_i = 0.2$, and $\delta = 0.1$, 0.2, 0.4, and 0.6. The inner droplet is on x axis. (a) $\delta = 0.1$, and $t = 0$, 0.1, 0.3, 1, 2, 3, and 5.08; (b) $\delta = 0.2$, and $t = 0$, 0.1, 0.3, 1, 2, and 4.98; (c) $\delta = 0.4$, and $t = 0$, 0.1, 0.3, 1, 2, 4, and 4.82; (d) $\delta = 0.6$, and $t = 0$, 0.1, 0.3, 1, 2, 3.5, and 4.

In Fig. 30, we investigate the transient deformation of eccentric compound droplets with constant parameters of $Ca_o = 0.10$, $k = 0.39$, $\Gamma = 0.5$, and $\lambda_o = \lambda_i = 0.2$. Concentric compound droplets that have the same parameters are unstable and will break up due to the contact of the two interfaces. The inner droplet is on the x axis and has the eccentricity of $\delta = 0.1$, 0.2, 0.4, and 0.6. Regardless of the eccentricity, all the deformation curves of the inner droplet are nearly coincident with each other and overlapped with the curve of $\delta = 0$ that is the deformation curve a concentric compound droplet. All the deformation curves of the outer droplet show the same behavior.

In Fig. 31, we plot the time evolution of the eccentric compound droplets profiles for $\delta = 0.1$, 0.2, 0.4, and 0.6. Both outer and inner droplets deform as they migrate in the negative x direction. The inner droplet migrates faster when the compound droplet has a larger eccentricity. At $t = 1$, all the inner droplets arrive at the stagnant point and stop moving. However, they deform rapidly at the same time. All the compound droplets eventually break up due to the contact of the two interfaces. It is interesting to notice that all the inner droplets reach the stagnant point and break up at nearly the same time regardless the eccentricity.

We also investigate eccentric compound droplets that have a small inner droplet. The compound droplets have constant parameters of $Ca_o = 0.10$, $k = 0.1$, $\Gamma = 0.5$, and $\lambda_o = \lambda_i = 0.2$. As mentioned in Section 4.1, the influence of an inner droplet is negligible when the inner droplet is sufficiently small. In this case, we want to investigate whether the eccentric compound droplet can reach steady state if the inner droplet is small. In Fig. 32, we present the plots of the deformation as a function of time for both inner and outer droplets. We observe that the deformation of both outer and inner droplets can reach a constant stage for the eccentric compound droplet that has different eccentricities, which indicates the eccentric compound droplet is able to

(a) inner
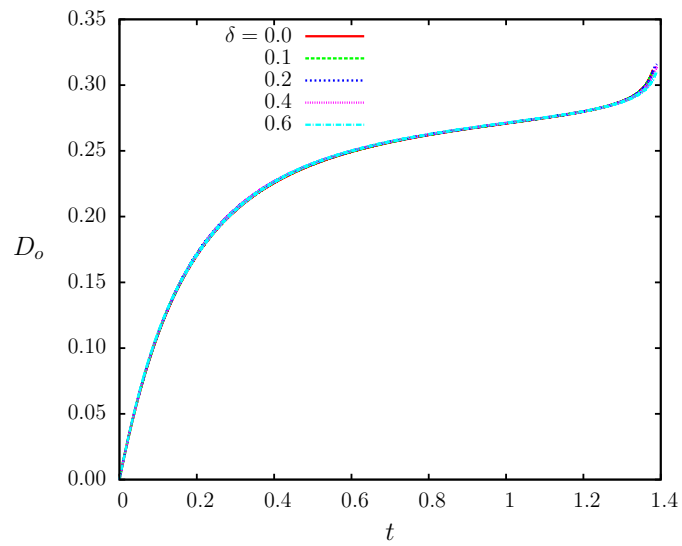
(b) outer

Figure 30: The influence of eccentricity on the deformation of the compound droplets for $Ca_o = 0.10$, $k = 0.39$, $\Gamma = 0.5$, $\lambda_o = \lambda_i = 0.2$, and $\delta = 0$, 0.1, 0.2, 0.4, and 0.6. The inner droplet is on the x axis.
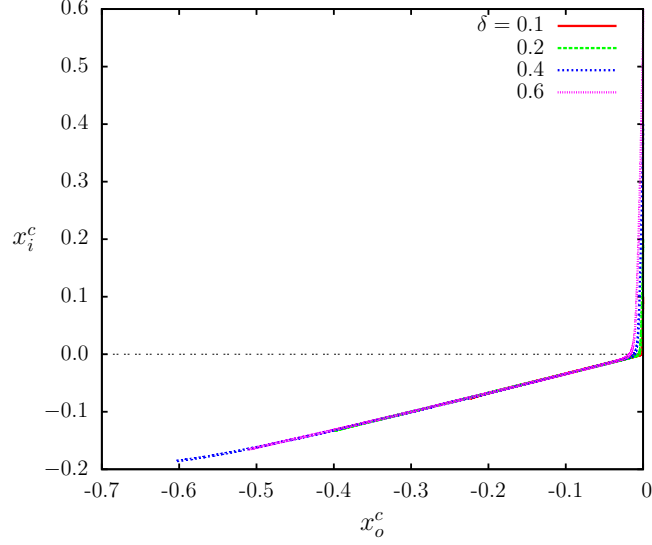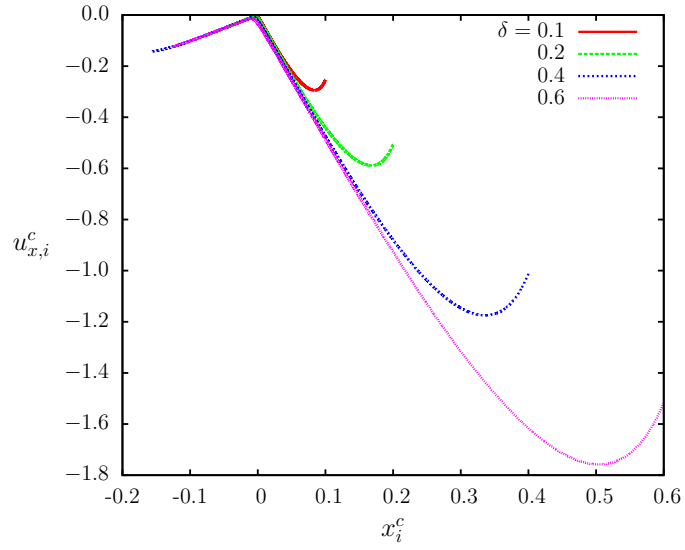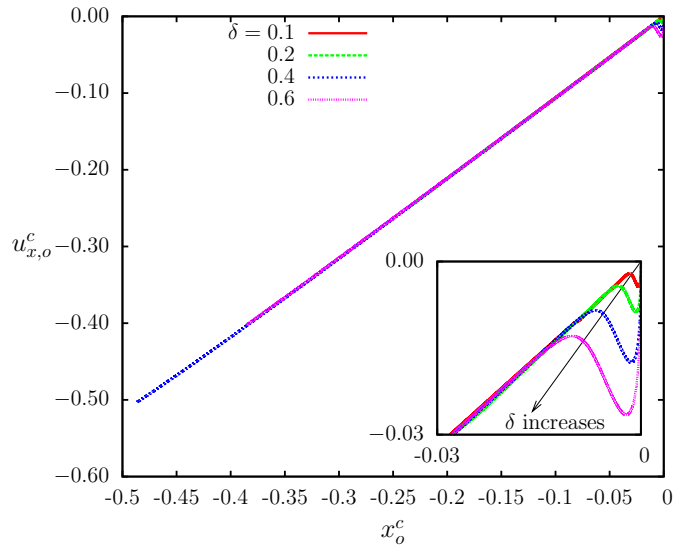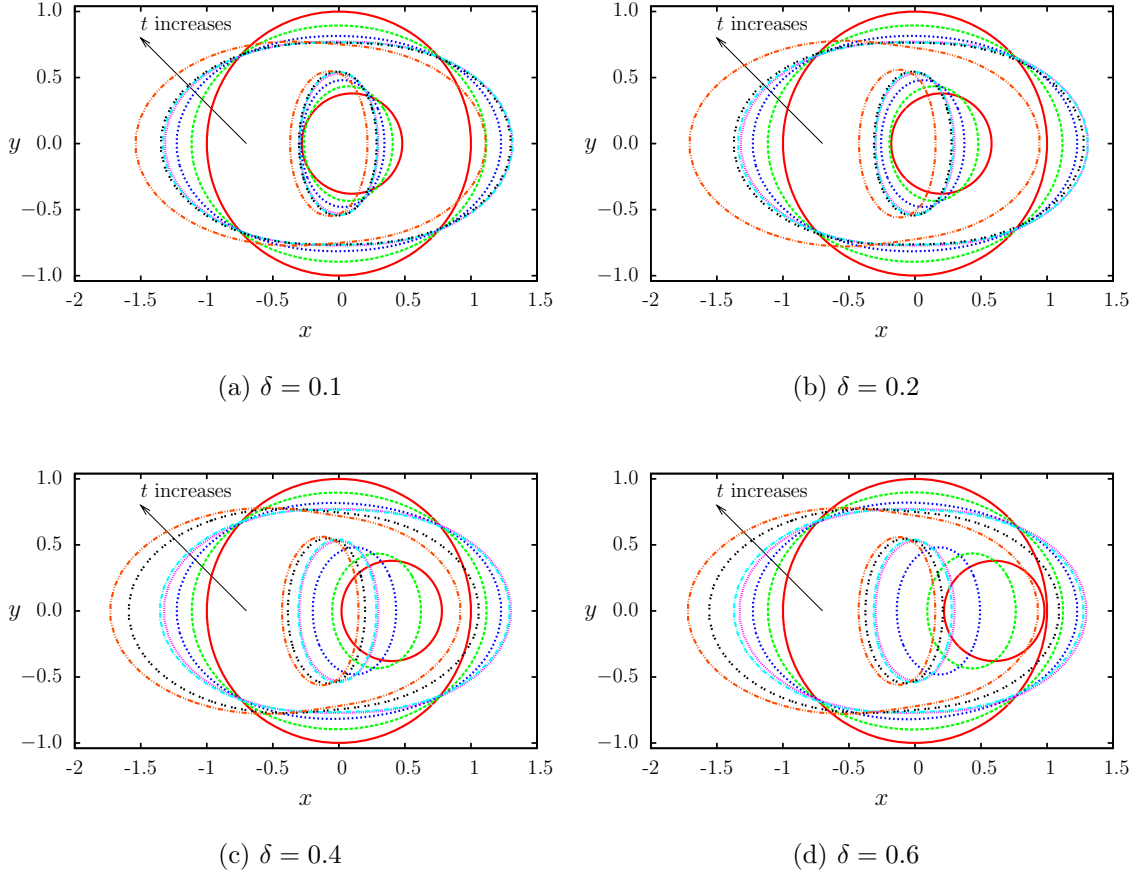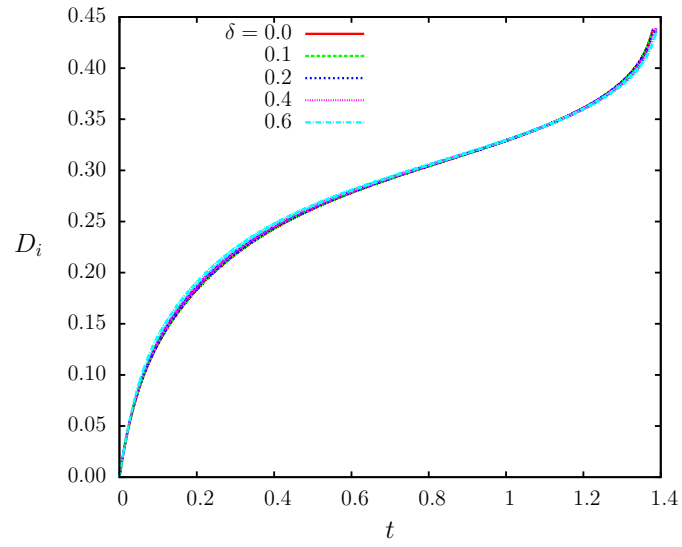
Figure 31: Time evolution of the eccentric compound droplets profiles on xy plane for $Ca_o = 0.10$, $k = 0.39$, $\Gamma = 0.5$, $\lambda_o = \lambda_i = 0.2$, and $\delta = 0.1$, 0.2, 0.4, and 0.6. The inner droplet is on x axis. (a) $\delta = 0.1$, and $t = 0$, 0.1, 0.3, 1, and 1.38; (b) $\delta = 0.2$, and $t = 0$, 0.1, 0.3, 1, and 1.38; (c) $\delta = 0.4$, and $t = 0$, 0.1, 0.3, 1, and 1.39; (d) $\delta = 0.6$, and $t = 0$, 0.1, 0.3, 1, and 1.39.

achieve the steady state when the inner droplet is small. For the inner droplet, the eccentricity slightly changes the transient deformation of the inner droplet when $\delta = 0.8$, but it does not influence the steady state deformation of the inner droplet. The eccentricity does not change the behavior of the outer deformation at all. All the steady state deformation of the eccentric compound droplet is the same with a concentric compound droplet that has the same flow properties and inner droplet size.

Fig. 33 shows the time evolution of the eccentric droplet profiles on xy plane for $Ca_o = 0.10$, $k = 0.1$, $\Gamma = 0.5$, $\lambda_o = \lambda_i = 0.2$, and $\delta = 0.1, 0.2, 0.4$, and 0.8. The inner droplet is farther from stagnant point when the eccentricity is larger. As time progresses, the inner droplet moves in the negative x direction. From $t = 0$ to 0.1, the inner droplet moves farther when the eccentricity is higher, which indicates that the inner droplet has a higher centroidal velocity. The outer droplet has relatively large deformation and elongates along x axis, while the inner droplet does not show much deformation. This is due to the fact that since the inner droplet is small, the inner capillary number is also small.

5.2. Internal droplet on y axis

In this case, we employ the same parameters of the eccentric compound droplet in Section 5.1, which are $Ca_o = 0.10$, $k = 0.38$, $\Gamma = 0.5$, and $\lambda_o = \lambda_i = 0.2$, except that the centroid of the inner droplet is initially placed on the positive y axis, thus its center of mass has a coordinate of $(0, \delta, 0)$.

Fig. 34 presents the y-component of the centroidal velocity (u_y^c) as a function of time. At the onset of the 2D extensional flow, all the inner droplets gains an initial centroidal velocity towards the positive y direction. When the eccentricity is larger, this initial centroidal velocity is higher, which implies that the flow near the outer interface is stronger than that around the stagnant point. The centroidal velocity
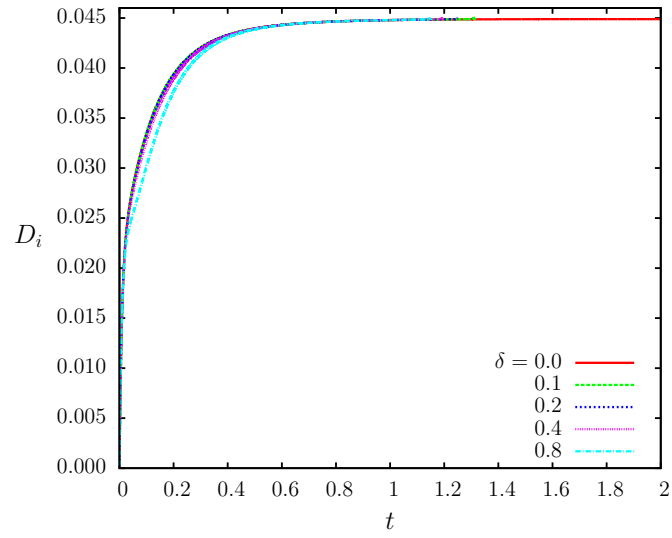
(a) inner
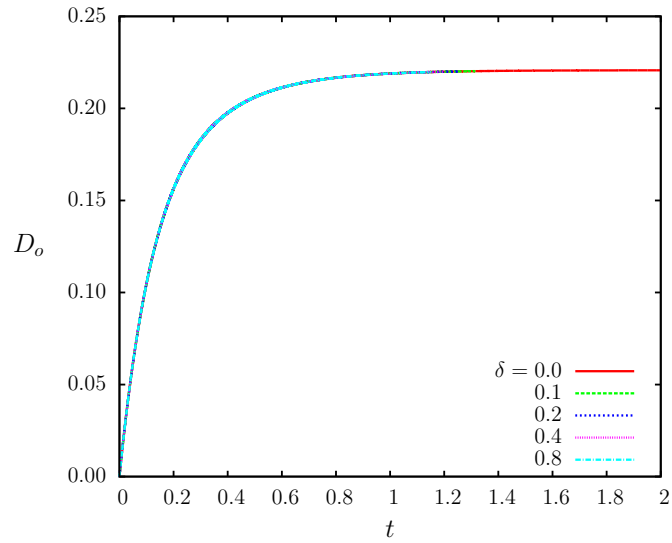
(b) outer

Figure 32: The influence of eccentricity on the deformation of the compound droplet. $Ca_o = 0.10$, $k = 0.1$, $\Gamma = 0.5$, $\lambda_o = \lambda_i = 0.2$, and $\delta = 0.1$, 0.2, 0.4, and 0.8. The inner droplet is on the x axis.
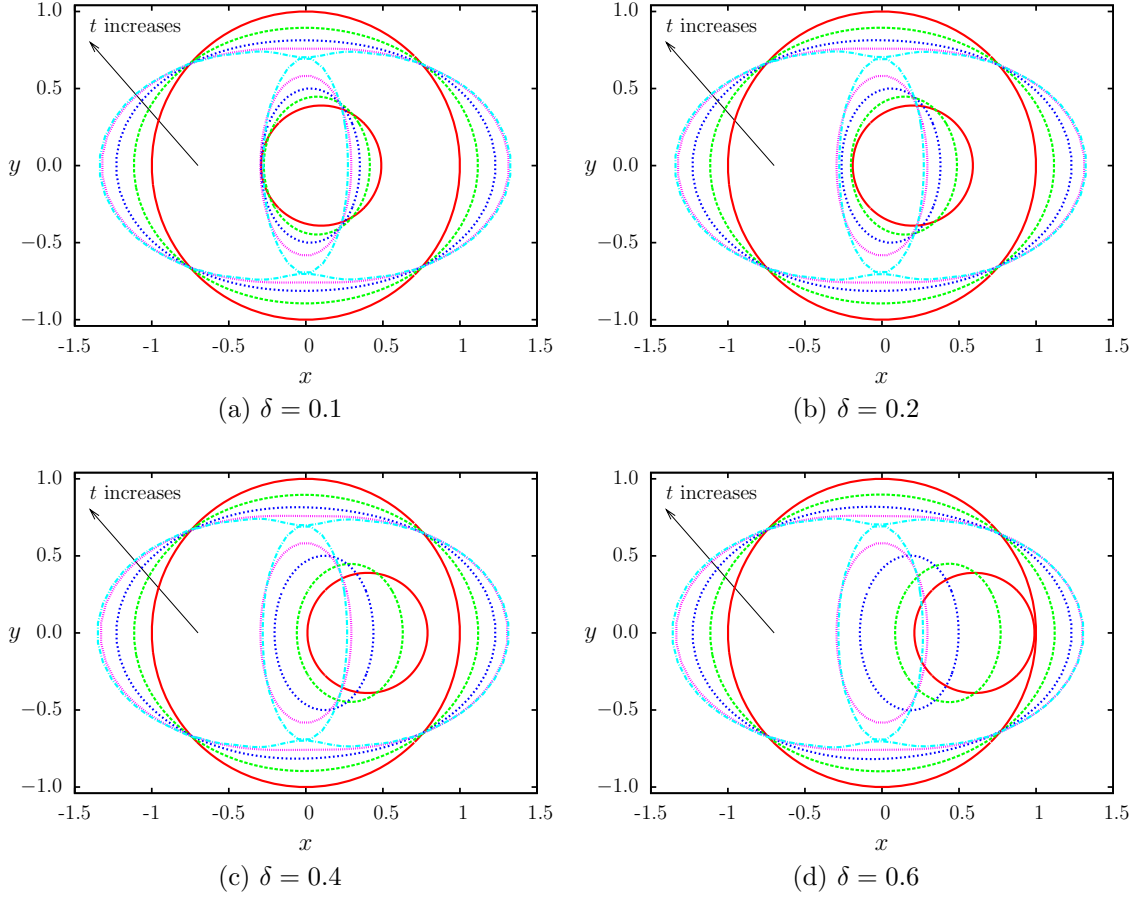
Figure 33: Time evolution of compound droplets profiles on xy plane for $Ca_o = 0.10$, $k = 0.1$, $\Gamma = 0.5$, $\lambda_o = \lambda_i = 0.2$, and $\delta = 0.1$, 0.2, 0.4, and 0.8. The inner droplet is on the x axis. (a) $\delta = 0.1$, and $t = 0$, 0.1, and 1.31; (b) $\delta = 0.2$, and $t = 0$, 0.1, and 1.25; (c) $\delta = 0.4$, and $t = 0$, 0.1, 0.2, 0.35, and 1.19; (d) $\delta = 0.8$, and $t = 0$, 0.1, 0.2, 0.35, and 1.14.

increases as the time progresses until the compound droplet breaks up. Since the centroidal velocity is in the positive direction, the inner droplet is moving towards the outer interface. The two interfaces contact each other quickly, which results in the breakup of the compound droplet. The motion of the inner droplet causes the outer droplet move in the positive y direction too, though the centroidal velocity of the outer droplet is negligible. When the inner droplet is on the y axis, The x and z components of the centroidal velocity are always zero, which indicates that the flow inside the outer droplet is symmetric along x and z axes.

In Fig. 35a, we present the time evolution of compound droplets profiles on xy plane for $\delta = 0.1$, 0.2, and 0.4. The compound droplet deforms and migrates at the same time. The inner droplet migrates quickly towards the outer interface, meanwhile, it elongates along y axis, which results in a quick breakup of the compound droplet. The compound droplet that has higher eccentricity breaks up earlier. This is not only because the initial distance between two interfaces is smaller, but also because the initial centroidal velocity of the inner droplet is higher.

In Fig. 36, we plot the transient deformation of the compound droplet. The compound droplet that has smaller eccentricity deforms longer and larger, which is due to the fact that it is farther from the outer interface. The deformation rate of both inner and outer droplets suddenly increases because of the strong interaction between the two interfaces.

5.3. Internal droplet on z axis

We also investigate the motion of compound droplets when the inner droplet starts to move with an initial location of $(0, 0, \delta)$. We still use the same fluid properties, except that the centroid of the inner droplet is initially placed on the z axis.

63
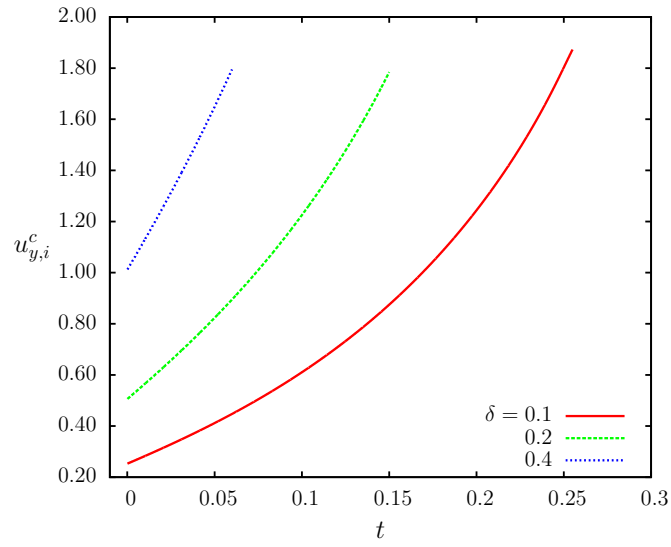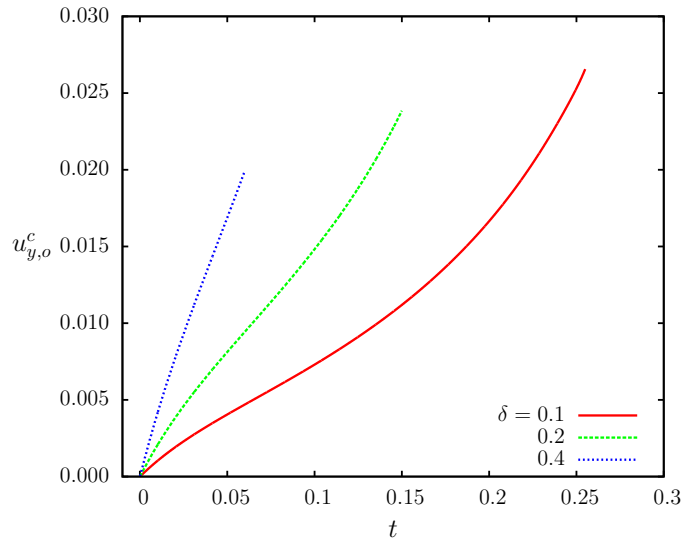
(a) inner

(b) outer

Figure 34: The influence of eccentricity on the y-component of the centroidal velocity for $Ca_o = 0.10$, $k = 0.38$, $\Gamma = 0.5$, $\lambda_o = \lambda_i = 0.2$, and $\delta = 0.1$, 0.2, and 0.4. The inner droplet is on the y axis.
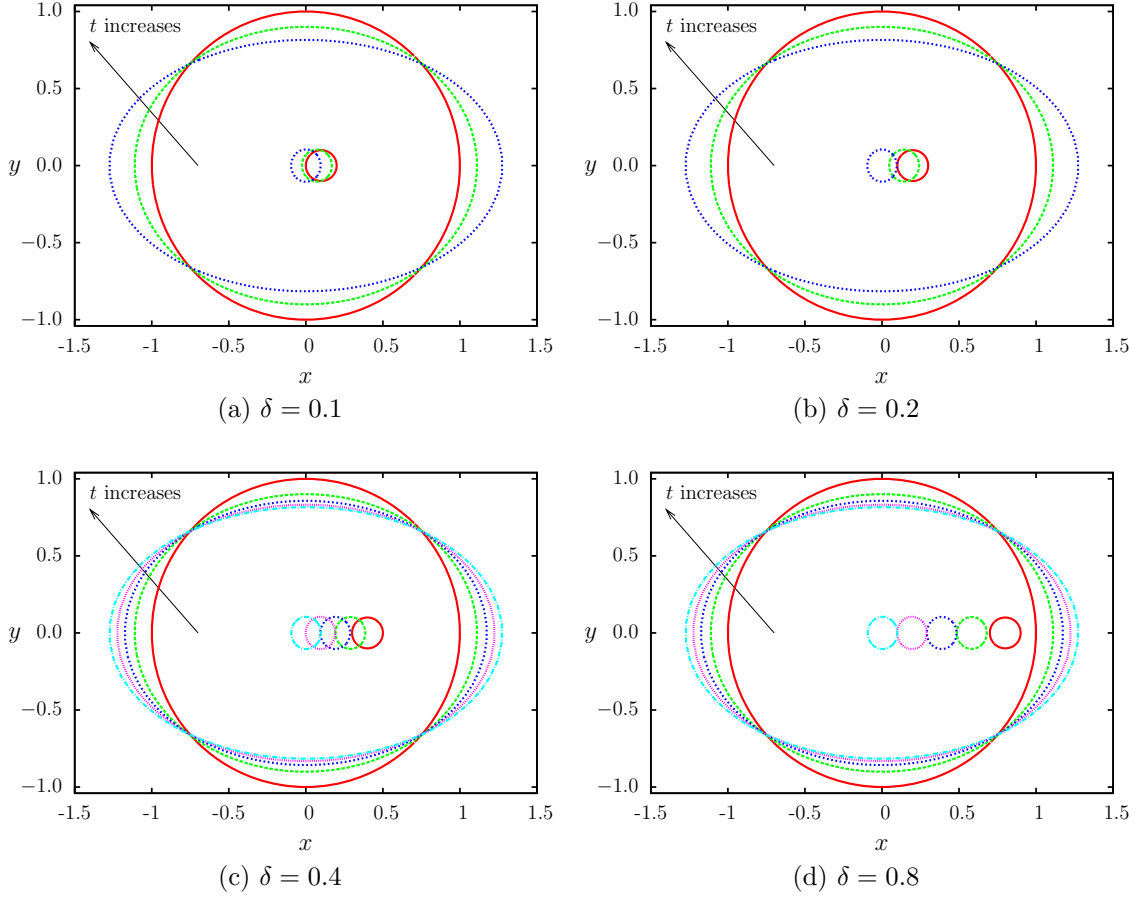
Figure 35: Time evolution of compound droplets profiles on xy plane for $Ca_o = 0.10$, $k = 0.38$, $\Gamma = 0.5$, $\lambda_o = \lambda_i = 0.2$, and $\delta = 0.1$, 0.2, and 0.4. The inner droplet is on the y axis. (a) $\delta = 0.1$, and $t = 0$, 0.1, 0.2, and 0.25; (b) $\delta = 0.2$, and $t = 0$, 0.1, and 0.16; (c) $\delta = 0.4$, and $t = 0$, and 0.06.
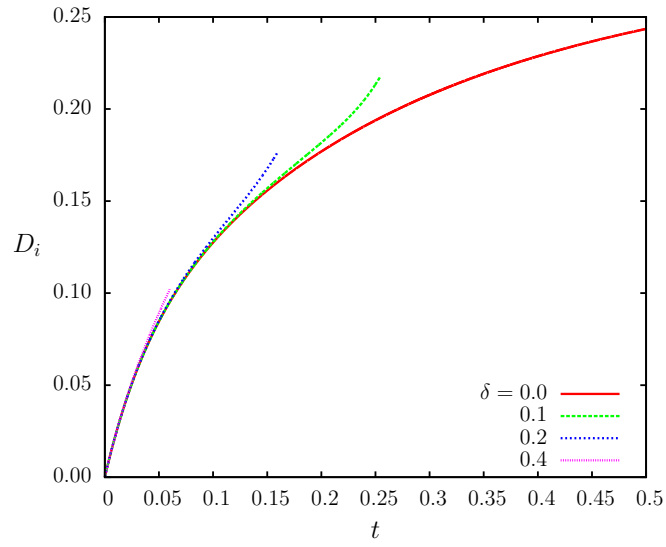
(a) inner
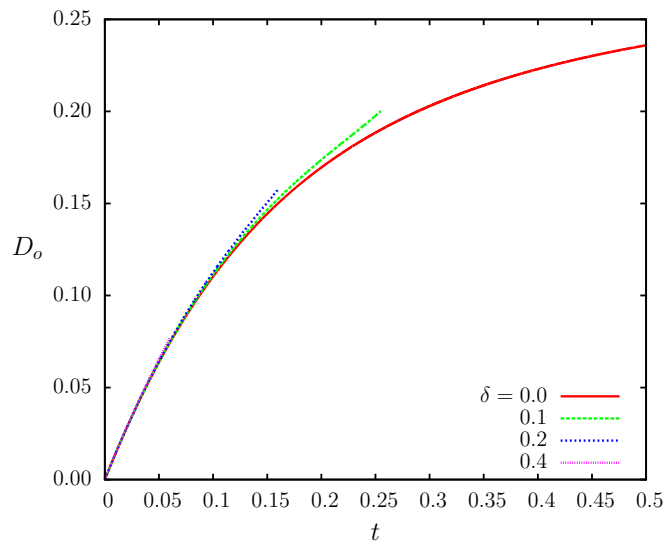
(b) outer

Figure 36: The influence of eccentricity on the deformation of the compound droplet for $Ca_o = 0.10$, $k = 0.38$, $\Gamma = 0.5$, $\lambda_o = \lambda_i = 0.2$, and $\delta = 0$, 0.1, 0.2, and 0.4. The inner droplet is on the y axis.

In Fig. 37, we present plots of the deformation as a function of time. When the eccentricity is larger, the deformation of the inner droplet when the inner droplet breaks up is larger, and the inner droplet breaks up earlier. The deformaiton of compound droplet with $\delta = 0.6$ is smaller than that of $\delta = 0.4$ because the former breaks up very fast due to the contact of the two interfaces. However, the eccentricity has insignificant influence on the deformation of the outer droplet. Fig. 38 shows the time evolution of the compound droplet profiles for $\delta = 0.1, 0.2, 0.4$, and 0.6. The flow inside the outer droplet elongates the inner droplet along y axis and bends the end of the inner droplet towards the outer interface. As the eccentricity increases, the inner droplet becomes more deformed due to the fact that the flow near the outer interface is stronger compared to the flow around the stagnant point. The inner droplet does no migrate at all due to the symmetry. When the inner droplet is initially placed on the z axis, the x and y components of the centroidal velocity are always zero.

5.4. Conclusion of eccentric compound droplets

In this chapter, we study the behavior of eccentric compound droplets freely suspended in a 2D extensional flow. We investigate the eccentric compound droplets that have their inner droplet on x, y, or z axis.

The eccentricity substantially increases the deformation of the inner droplet and causes the inner droplet break up. However, its influence on the deformation of the outer droplet is insignificant. Regardless of the eccentricity and position of the inner droplet, the behavior of the outer droplet's deformation is close to that of the concentric compound droplet.

We know that when the inner droplet is place on either x, y, or z axis, the flow inside the outer droplet is symmetric along the other two axes. The flow field is strong near the outer interface and weak around the stagnant point. The 2D extensional flow elongates the outer droplet along x axis, and the recirculating flow inside elongates the

67
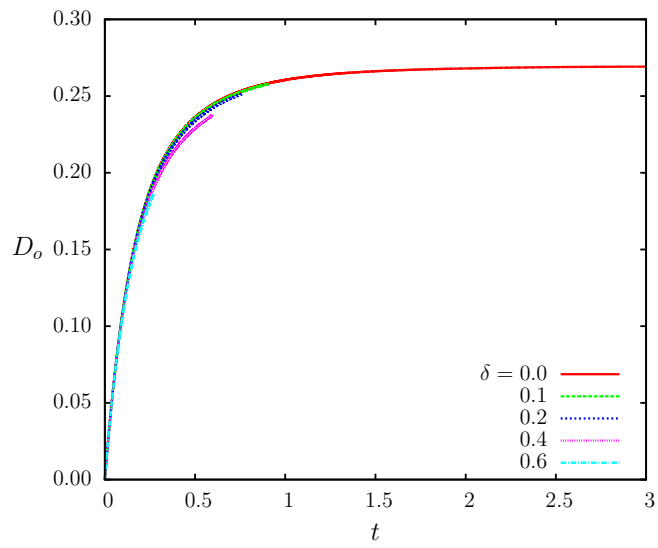
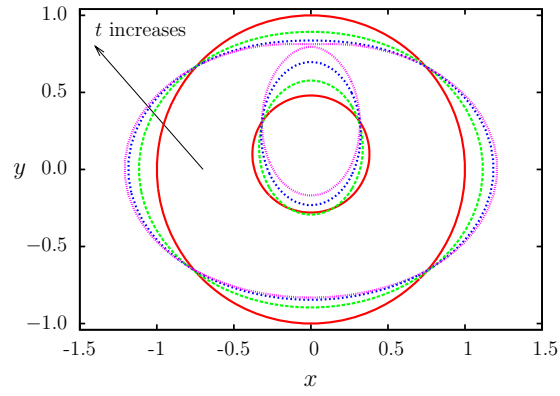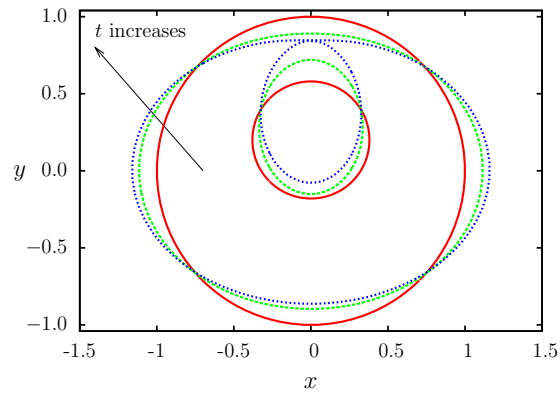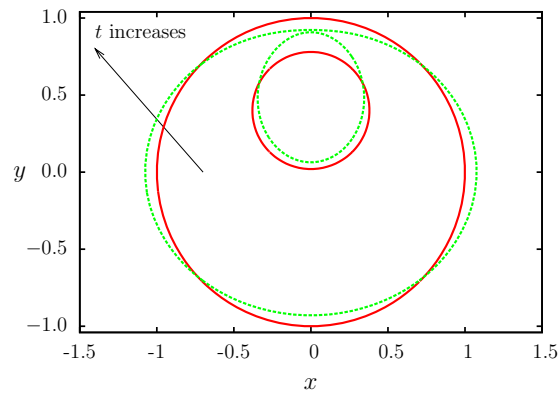(a) inner

(b) outer

Figure 37: The influence of eccentricity on the deformation of the compound droplets. $Ca_o = 0.10$, $k = 0.38$, $\Gamma = 0.5$, $\lambda_o = \lambda_i = 0.2$, and $\delta = 0.1$, 0.2, 0.4,and 0.6. The inner droplet is placed on the z axis.
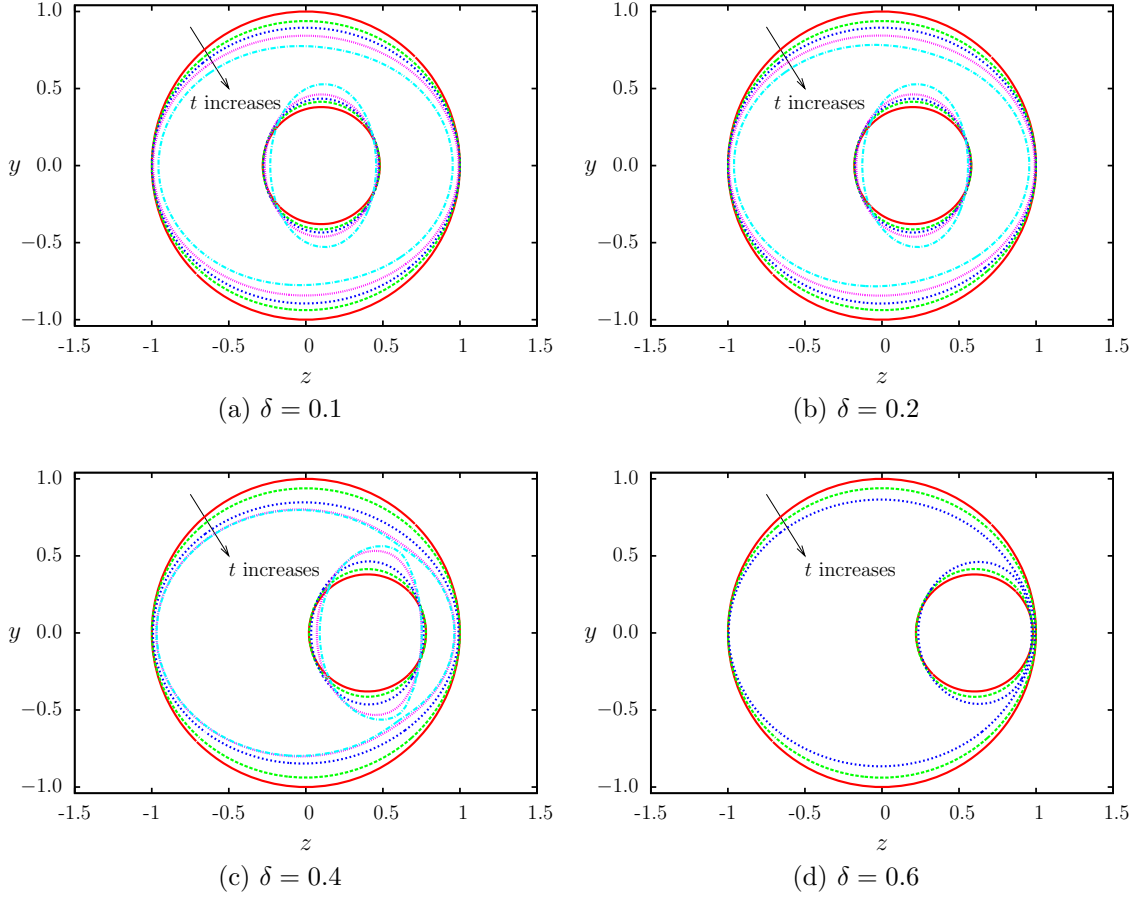
Figure 38: Time evolution of compound droplets profiles on zy plane for $Ca_o = 0.10$, $k = 0.38$, $\Gamma = 0.5$, $\lambda_o = \lambda_i = 0.2$, and $\delta = 0.1, 0.2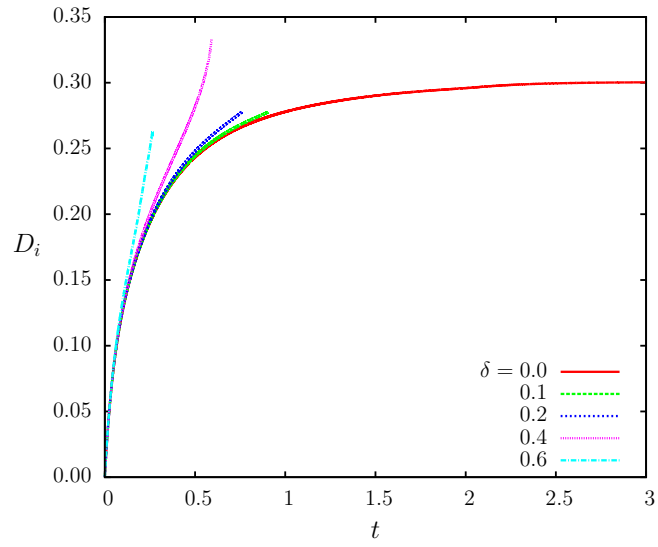, 0.4$, and 0.6. The inner droplet is on the z axis. (a) $\delta = 0.1$, and $t = 0, 0.05, 0.1, 0.2$, and 0.9; (b) $\delta = 0.2$, and $t = 0$, $0.05, 0.1, 0.2$, and 0.75; (c) $\delta = 0.4$, and $t = 0, 0.05, 0.2, 0.5$, and 0.58; (d) $\delta = 0.6$, and $t = 0, 0.05$, and 0.16.

69

inner droplet along the y axis. This behavior is the same as a concentric compound droplet. When the inner droplet is placed on the z axis, the internal flow bends the ends of the inner droplet towards the outer interface.

When the inner droplet is initially placed on the x axis, it moves towards the stagnant point. There are three possible final states of the inner droplet. It may pass the stagnant point and break up by itself. It may contact the outer interface due to large deformation and break up together with the outer droplet. When its size is small, it can stop at the stagnant point and reach the steady state. When the inner droplet is initially placed on the y axis, it moves towards the outer interface, which will cause the contact of the two interfaces and the breakup of the compound droplet. When the inner droplet is initially on the z axis, it does not migrate, but its bended end may contact the outer interface and cause the compound droplet to break up.

CHAPTER 6. CONCLUSION

In this work, we employ a three-dimensional spectral boundary element method to investigate the behavior and stability of compound droplets in a two-dimensional extensional flow. Firstly, we validate our numerical scheme in Chapter 3 and compare our numerical results with Stone and Leal's work [40]. All results show good agreement which indicates that our numerical scheme can be applied to simulate the behavior of compound droplets.

Secondly, in Chapter 4, we investigate the behavior and stability of concentric compound droplets and the three major parameters that affect them. These three parameters are size ratio, surface tension ratio, and viscosity ratios. A two-dimensional extensional flow deforms the outer droplet into a prolate spheroidal shape that its longest axis is along x axis, while the recirculating flow inside the outer droplet deforms the inner droplet into a prolate spheroidal shape that its longest axis is along y axis. The inner droplet size has substantial influence on the deformation and stability of compound droplets. As it increases, the deformation of both inner and outer droplets increases. When it exceeds a critical value, the compound droplet breaks up. The critical size ratio decreases as the outer capillary number increases. However, if the inner droplet size is very small, like $k = 0.1$, its influence on the outer droplet is negligible. The surface tension ratio mainly influences the deformation of the inner droplet. As it increases, the deformation of the inner droplets increases dramatically. We also found critical values for the surface tension ratio, below which the compound droplet breaks up. The critical surface tension ratio increases as the outer capillary number increases. The increase of the inner viscosity ratio significantly decreases the deformation of the compound droplet, while the increase of the outer viscosity ratio substantially increases the deformation of the compound droplet. When the inner viscosity ratio increases, it can stabilize the compound droplet. The increase of the

71

outer viscosity has different influence on the stability of the compound droplet within different range of the inner viscosity ratio. When $\lambda_i \ll 1$, it increases the stability of the compound droplet; when $\lambda_i = O(1)$, it decreases the stability of the compound droplet. The breakup of the compound droplet could be due to the contact of the two interfaces. When both surface tension ratio and outer capillary number are small such as $Ca_o = 0.01$ and $\Gamma = 0.3$, the inner droplet breaks up without contact the outer interface, while, at the same time, the outer droplet does not deform very much.

Finally, in Chapter 5, we study the behavior of eccentric compound droplets. The eccentricity has substantial influence on the inner droplet and little influence on the outer droplet deformation. When the inner droplet is initially placed on either x, y, or z axis, the flow inside the outer droplet is symmetric along the other two axes. The 2D extensional flow elongates the outer droplet along x axis, and the recirculating flow inside elongates the inner droplet along the y axis. This behavior is similar to concentric compound droplets. When the inner droplet is initially placed on the z axis, the internal flow bends the ends of the inner droplet towards the outer interface at the same time. When the inner droplet is initially placed on the x axis, it moves towards the stagnant point. When the inner droplet is initially placed on the y axis, it moves towards the outer interfaces. When it is initially on the z axis, it does not move. The outer droplet always moves in the same direction as the inner droplet. The breakup of eccentric compound droplets could be due to the contact of the two interfaces or the breakup of the inner droplet.

REFERENCES

[1] N. Akhtar, M. Ahmad, H. M. S. Khan, J. Akram, Gulfishan, A. Mahmood, and M. Uzair, *Formulation and characterization of a multiple emulsion containing 1% L-ascorbic acid*, Bulletin of the Chemical Society of Ethiopia **24** (2010), 1–10.

[2] N. Akhtar and Y. Yazan, *Formulation and in-vivo evaluation of a cosmetic multiple emulsion containing vitamin C and wheat protein*, Pakistan Journal of Pharmaceutical Sciences **21** (2008), 45–50.

[3] E. P. Ascoli, D. S. Dandy, and L. G. Leal, *Low Reynolds number hydrodynamic interaction of a solid particle with a planar wall*, International Journal for Numerical Methods in Fluids **9** (1989), 651–688.

[4] A. Benichou, A. Aserin, and N. Garti, *Double emulsions stabilized by new molecular recognition hybrids of natural polymers*, Polymers for Advanced Technologies **13** (2002), 1019–1031.

[5] A. Benichou, A. Aserin, and N. Garti, *Double emulsions stabilized with hybrids of natural polymers for entrapment and slow release of active matters*, Advances in Colloid and Interface Science **108-109** (2004), 29–41.

[6] L. Boyadzhiev and E. Bezenshek, *Carrier mediated extraction: application of double emulsion technique for mercury removal from waste water*, Journal of Membrane Science **14** (1983), 13–18.

[7] L. Boyadzhiev, E. Bezenshek, and Z. Lazarova, *Removal of phenol from waste water by double emulsion membranes and creeping film pertraction*, Journal of Membrane Science **21** (1984), no. 2, 137–144.

[8] A. F. Brodin and S. G. Frank, *Drug release from o/w/o multiple emulsion systems*, Acta Pharmaceutica Suecica **15** (1978), 111–118.

[9] L. Y. Chu, A. S. Utada, R. K. Shah, J. W. Kim, and D. A. Weitz, *Controllable monodisperse multiple emulsions*, Angewandte Chemie **119** (2007), 9128–9132.

[10] A. M. J. Davis and H. Brenner, *Emulsions containing a third solid internal phase*, Journal of the Engineering Mechanics Division **107** (1981), 609–621.

[11] E. Dickinson, *Double emulsions stabilized by food biopolymers*, Food Biophysics **6** (2011), 1–11.

[12] I. Egry, *The oscillation spectrum of a compound drop*, Journal of Materials Science **40** (2005), 2239–2243.

[13] A. T. Florence and D. Whitehill, *The formulation and stability of multiple emulsions*, International Journal of Pharmaceutics **11** (1982), 227.

[14] N. Garti, M. Frenkel, and R. Shwartz, *Multiple emulsions: Part II: Proposed technique to overcome unpleasant taste of drugs*, Journal of Dispersion Science and Technology **4** (1983), 237–252.

[15] J. A. Hanson, C. B. Chang, S. M. Graves, Z. Li, T. G. Mason, and T. J. Deming, *Nanoscale double emulsions stabilized by single-component block copolypetides*, Nature **455** (2008), 85–88.

[16] J. J. L. Higdon and G. P. Muldowney, *A spectral boundary element approach for the three dimensional Stokes equations applied to free surface flows*, Transactions on Modelling and Simulation **10** (1995), 605–612.

[17] H. C. Kan, W. Shyy, H. S. Udaykumar, P. Vigneron, and R. Tran-Son-Tay, *Effects of nucleus on leukocyte recovery*, Annals of Biomedical Engineering **27** (1999), 648–655.

[18] H. C. Kan, H. S. Udaykumar, W. Shyy, and R. Tran-Son-Tay, *Hydrodynamics of a compound drop with application to leukocyte modeling*, Physics of Fluids **10** (1998), 760–774.

[19] H. C. Kan, H. S. Udaykumar, W. Shyy, and R. Tran-Son-Tay, *Numerical analysis of the deformation of an adherent drop under shear flow*, Journal of Biomechanical Engineering **121** (1999), 160–169.

[20] D. B. Khismatullin and G. A. Truskey, *Three-dimensional numerical simulation of receptor-mediated leukocyte adhesion to surfaces: Effects of cell deformability and viscoelasticity*, Physics of Fluids **17** (2005), 032505.

[21] K. A. Landman, *Stability of a viscous compound fluid drop*, AiChE Journal **31** (1985), 567–573.

[22] C. P. Lee, A. V. Anilkumar, and T. G. Wang, *A theoretical model for centering of a thin viscous liquid shell in free and forced capillary oscillations*, Physics of fluids **8** (1996), 2580–2589.

[23] D. J. McClements, *Food Emulsions: Principles, Practices, and Techniques*, CRC Press, Boca Raton, 2005.

[24] G. Muschiolik, *Multiple emulsions for food use*, Current Opinion in Colloid and Interface Science **12** (2007), 213–220.

[25] T. Nisisako, *Microstructured devices for preparing controlled multiple emulsions*, Chemical Engineering and Technology **31** (2008), 1091–1098.

[26] H. Okochi and M. Nakano, *Basic studies on formulation, method of preparation and characterization of water-in-oil-in-water type multiple emulsions containing vancomycin*, Chemical and Pharmaceutical Bulletin **44** (1996), 180–186.

[27] V. Pappu and P. Bagchi, *3D computational modeling and simulation of leukocyte rolling adhesion and deformation*, Computers in Biology and Medicine **38** (2008), 738–753.

[28] M. Paye, A. O. Barel, and H. I. Maibach, *Handbook of cosmetic science and technology*, CRC Press, Florida, 2006.

[29] K. Pays, J. Giermanska-Kahn, B. Pouligny, J. Bibette, and F. Leal-Calderon, *Double emulsions: how does release occur?*, Journal of Controlled Release **79** (2002), 193–205.

[30] C. Pozrikidis, *Boundary integral and singularity methods for linearized viscous flow*, Combridge University Press, New York, 1992.

[31] C. Prybilski, M. D. Luca, J. L. Grossiord, C. Vaution, and M. Seiller, *W/O/W multiple emulsions: Manufacturing and formulation considerations*, Cosmetics and Toiletries **106** (1991), 97–100.

[32] X. Qi, L. Wang, and J. Zhu, *Water-in-oil-in-water double emulsions: An excellent delivery system for improving the oral bioavailability of pidotimod in rats*, Journal of Pharmaceutical Sciences **100** (2011), 2203–2211.

[33] E. Rushton and G. A. Davies, *Settling of encapsulated droplets at low Reynolds numbers*, International Journal of Multiphase Flow **9** (1983), 337–342.

[34] S. S. Sadhal and R. E. Johnson, *Stokes flow past bubbles and drops partially coated with thin films. Part 1. Stagnant cap of surfactant film - exact solution*, Journal of Fluid Mechanics **126** (1983), 237–250.

[35] S. S. Sadhal and H. N. Oguz, *Stokes flow past compound multiphase drops: the case of completely engulfed drops/bubbles*, Journal of Fluid Mechanics **160** (1985), 511–529.

[36] L. Sapei, M. A. Naqvi, and D. Rousseau, *Stability and release properties of double emulsions for food applications*, Food Hydrocolloids **27** (2012), 316–323.

[37] W. Seifriz, *Studies in emulsions*, The Journal of Physical Chemistry **29** (1925), 738–749.

[38] R. K. Shah, H. C. Shum, A. C. Rowat, D. Lee, J. J. Agresti, A. S. Utada, L. Y. Chu, J. W. Kim, A. Fernandez-Nieves, C. Martinez, and D. A. Weitz, *Designer emulsions using microfluidics*, Materialstoday **11** (2008), 18–27.

[39] K. A. Smith, J. M. Ottino, and M. Olvera de la Cruz, *Encapsulated drop breakup in shear flow*, Physical Review Letters **93** (2004), 204501.

[40] H. A. Stone and L. G. Leal, *Breakup of concentric double emulsion droplets in linear flows*, Journal of Fluid Mechanics **211** (1990), 123–156.

[41] S. Tasoglu, G. Kaynak, A. J. Szeri, U. Demirci, and M. Muradoglu, *Impact of a compound droplet on a flat surface: A model for single cell epitaxy*, Physics of Fluids **22** (2010), 082103.

[42] S. Torza and S. G. Mason, *Three-phase interactions in shear and electrical fields*, Journal of Colloid and Interface Science **33** (1970), 67–83.

[43] P. B. Umbanhowar, V. Prasad, and D. A. Weitz, *Monodisperse emulsion generation via drop break off in a coflowing stream*, Langmuir **16** (2000), 347–351.

[44] A. S. Utada, E. Lorenceau, D. R. Link, P. D. Kaplan, H. A. Stone, and D. A. Weitz, *Monodisperse double emulsions generated from a microcapillary device*, Science **308** (2005), 537–541.

[45] F. Valenzuela, C. Fonseca, C. Basualto, O. Correa, C. Tapia, and J. Sapag, *Removal of copper ions from a waste mine water by a liquid emulsion membrane method*, Minerals Engineering **18** (2005), 33–40.

[46] Q. Wang, G. Tan, L. B. Lawson, V. T. John, and K. D. Papadopoulos, *Liposomes in double-emulsion globules*, Langmuir **26** (2010), no. 5, 3225–3231.

[47] Y. Wang, *Numerical studies of stokes flow in confined geometries*, Master's thesis, University of Maryland, 2004.

[48] Y. Wang and P. Dimitrakopoulos, *A three-dimensional spectral boundary element algorithm for interfacial dynamics in Stokes flow*, Physics of fluids **18** (2006), 082106.

[49] M. I. Younis, *MEMS linear and nonlinear statics and dynamics*, Springer, New York Dordrecht Heidelberg London, 2011.